



University of Kentucky
UKnowledge

Theses and Dissertations--Chemical and
Materials Engineering

Chemical and Materials Engineering

2017

FUNCTIONALIZATION OF SILVER NANOPARTICLES ON MEMBRANES AND ITS INFLUENCE ON BIOFOULING

Conor G. Sprick

University of Kentucky, cgsprick@gmail.com

Author ORCID Identifier:

<https://orcid.org/0000-0002-1306-3460>

Digital Object Identifier: <https://doi.org/10.13023/ETD.2017.331>

[Right click to open a feedback form in a new tab to let us know how this document benefits you.](#)

Recommended Citation

Sprick, Conor G., "FUNCTIONALIZATION OF SILVER NANOPARTICLES ON MEMBRANES AND ITS INFLUENCE ON BIOFOULING" (2017). *Theses and Dissertations--Chemical and Materials Engineering*. 77. https://uknowledge.uky.edu/cme_etds/77

This Master's Thesis is brought to you for free and open access by the Chemical and Materials Engineering at UKnowledge. It has been accepted for inclusion in Theses and Dissertations--Chemical and Materials Engineering by an authorized administrator of UKnowledge. For more information, please contact UKnowledge@lsv.uky.edu.

STUDENT AGREEMENT:

I represent that my thesis or dissertation and abstract are my original work. Proper attribution has been given to all outside sources. I understand that I am solely responsible for obtaining any needed copyright permissions. I have obtained needed written permission statement(s) from the owner(s) of each third-party copyrighted matter to be included in my work, allowing electronic distribution (if such use is not permitted by the fair use doctrine) which will be submitted to UKnowledge as Additional File.

I hereby grant to The University of Kentucky and its agents the irrevocable, non-exclusive, and royalty-free license to archive and make accessible my work in whole or in part in all forms of media, now or hereafter known. I agree that the document mentioned above may be made available immediately for worldwide access unless an embargo applies.

I retain all other ownership rights to the copyright of my work. I also retain the right to use in future works (such as articles or books) all or part of my work. I understand that I am free to register the copyright to my work.

REVIEW, APPROVAL AND ACCEPTANCE

The document mentioned above has been reviewed and accepted by the student's advisor, on behalf of the advisory committee, and by the Director of Graduate Studies (DGS), on behalf of the program; we verify that this is the final, approved version of the student's thesis including all changes required by the advisory committee. The undersigned agree to abide by the statements above.

Conor G. Sprick, Student

Dr. Isabel Escobar, Major Professor

Dr. Thomas Dziubla, Director of Graduate Studies

FUNCTIONALIZATION OF SILVER NANOPARTICLES
ON MEMBRANES AND ITS INFLUENCE ON BIOFOULING

THESIS

A Thesis submitted in partial fulfillment of the requirements for
the degree of Master of Science in Materials Science & Engineering in the
College of Engineering
at the University of Kentucky

By

Conor Gary Lee Sprick

Lexington, Kentucky

Director: Dr. Isabel Escobar, Professor of Chemical and Materials Engineering

Lexington, Kentucky

2017

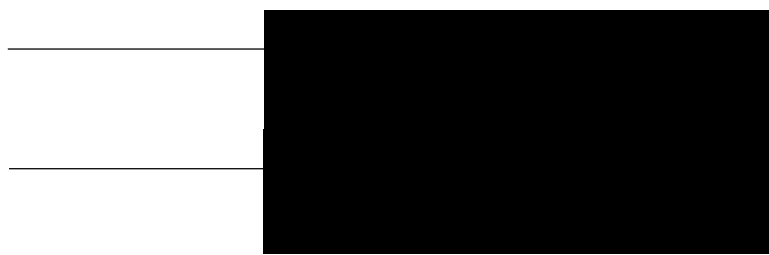
Copyright © Conor Gary Lee Sprick 2017

ABSTRACT OF THESIS

FUNCTIONALIZATION OF SILVER NANOPARTICLES ON MEMBRANES AND ITS INFLUENCE ON BIOFOULING

Ultrafiltration (UF) processes are often used as pretreatment before more retentive/costly processes, such as nanofiltration and reverse osmosis. This study shows the results of low-biofouling nanocomposite membranes, loaded with casein-coated silver nanoparticles (casein-Ag-NPs). Membranes were cast and imbedded with Ag-NPs using two approaches, physical blending of Ag-NPs in the dope solution (^PAg-NP/CA membranes) and chemical attachment of Ag-NPs to cast membranes (^CAg-NP/CA membranes), to determine their biofouling control properties. The functionalization of Ag-NPs onto the CA membranes was achieved via attachment with functionalized thiol groups with the use of glycidyl methacrylate (GMA) and cysteamine chemistries. The immobilization chemistry successfully prevented leaching of silver nanoparticles during cross-flow studies. *Pseudomonas fluorescens* Migula in brackish water was used for short-term dead-end filtration, where CA and ^CAg-NP/CA membranes displayed lower flux declines as compared to ^PAg-NP/CA membranes. In subsequent long-term biofouling studies, also with *Pseudomonas fluorescens* Migula in brackish water with addition of sodium acetate, chemically-attached Ag-NPs led to a significant reduction in the accumulation of bacterial cells, likely due to the more dispersed nanoparticles across the surface. Therefore, a method was developed to chemically immobilize Ag-NPs to membranes without losing Ag-NP's antimicrobial properties.

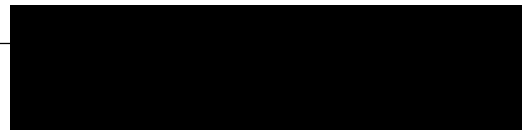
KEYWORDS: Silver Nanoparticles, Biofouling, Leaching, Ultrafiltration, Cellulose Acetate, *Pseudomonas fluorescens* Migula



FUNCTIONALIZATION OF SILVER NANOPARTICLES ON MEMBRANES AND
ITS INFLUENCE ON BIOFOULING

By

Conor Gary Lee Sprick



Dr. Thomas Dziubla

Director of Graduate Studies

July 10th, 2017

ACKNOWLEDGMENTS

These past two years at University of Kentucky had been some of the best years of my life. I have met and made many new lifelong friends with memories I will never forget. With sincere acknowledgment, I want to thank my advisor Dr. Isabel Escobar for letting me in your research group and for all the wisdom you have given me. Your constant feedback, encouragement and will for others to succeed has contributed so much. I also want to thank Dr. Dibakar Bhattacharyya and Dr. Gail Brion for your constant help and encouragement to help me reach my goals. Thank you both for serving on my committee.

I want to give my sincere thanks to all my friends and colleague from my research group: Xiaobo (Max) Dong, Dr. Sneha Chede, Priyesh Wagh, and Joyner Eke. All of you have contributed so much towards my success and achievements. You guys made it a pleasure for me to come in and do research every day. Even when times were rough, you guys had my back. Thank you so much. I also want to thank both my research undergraduates, T. Jaye McCalla and Christian Kuethe, for helping me. In addition, I want to thank Matt Hancock and Landon Motts for being such great friends and roommates and cheering me up whenever there were rough times.

In addition, I want to thank everyone from Dr. Dibakar Bhattacharyya's research group: Andrew Colburn, Michael Detisch, Sebastian Hernandez, Hongyi Wan, Ashish Aher, Madison Sloan, Saiful Islam, Rupam Sarma and Anthony Saad. Each and every one of you have helped in some way and made it a joy to go to lab every day.

Too many thanks go out towards my family and girlfriend. You guys encouraged me to keep pushing forward, even when it got too hard. Thank you, Tammy, for your love, patience and continuous support. Thank you, Mom, Dad, Grandpa, Grandma, Caitlyn, Logan and little Oaklyn, for always believing in me and allowing me to pursue my goals. I can never thank you guys enough for all your love and continuous support that I have had in my life. I want to dedicate this research work to my grandpa and grandma, Bill and Barb Sprick. You guys have taught me many valuable life lessons: family always come first, do your hardest and always cherish those around you.

TABLE OF CONTENTS

ACKNOWLEDGEMENT	iii
LIST OF TABLES.....	vii
LIST OF FIGURES	ix
1 INTRODUCTION	1
2 LITERATURE REVIEW	
2.1 Membranes	
2.1.1 Membrane Separation Mechanisms.....	5
2.1.2 Membrane Formation.....	8
2.1.3 Membrane Materials	9
2.2 Fouling	
2.2.1 Types of Fouling.....	10
2.2.2 Fouling Control.....	13
2.3 Silver Nanoparticles	
2.3.1 Properties of Silver Nanoparticles	15
2.3.2 Silver Nanoparticle Stabilizers	17
2.3.3 Chemical and Physical Functionalization of Silver Nanoparticles to Surfaces	18
2.3.4 Incorporation of Silver Nanoparticles onto Cellulose Acetate Membranes	19
3 OBJECTIVES	
3.1 Characterization of the Ag-NPs.....	21
3.2 Physical Attachment of the Ag-NPs	21
3.3 Chemical Attachment of Ag-NPs (^C Ag-NP/CA) onto the Membranes.....	21
3.4 Characteristics of the CA, ^P Ag-NP/CA and ^C Ag-NP/CA Membranes.....	22

3.5 Effects of Biofouling on CA, ^P Ag-NP/CA and ^C Ag-NP/CA Membranes.....	22
4 MATERIALS AND METHODS	
4.1 Materials	
4.1.1 Glassware.....	23
4.1.2 Chemical Reagents.....	23
4.1.3 Silver Nanoparticles (Ag-NPs)	23
4.1.4 Bacterial Analyses Materials	23
4.2 Methods	
4.2.1 Polymerization of GMA	24
4.2.2 Membrane Casting.....	26
4.2.3 Fabrication of Cellulose Acetate (CA) Membranes.....	26
4.2.4 Fabrication of Physically Attached Ag-NPs (^P Ag-NP)/CA Membranes	26
4.2.5 Fabrication of CA/GMA Membranes	27
4.2.6 Fabrication of Chemically Attached Ag-NPs (^C Ag-NP)/CA Membranes	27
4.3 Chemical and Morphological Characterization	
4.3.1 Transmission Electron Microscope.....	28
4.3.2 Fourier Transform Infrared (FTIR) Spectroscopy Analysis	28
4.3.3 X-ray Photoelectron Spectroscopy	29
4.3.4 Scanning Electron Microscope/Energy-dispersive X-ray Spectroscopy.....	29
4.3.5 Contact Angle	29
4.4 Permeability, Selectivity and Fouling Studies	
4.4.1 Bacteria Growth and Harvesting.....	30
4.4.2 Permeability Studies	30
4.4.3 Salt Rejection.....	32
4.4.4 Silver Leaching Crossflow Studies.....	32
4.4.5 48-Hour Biofouling Studies.....	34

4.4.6	Fluorescence Microscopy	34
5	RESULTS AND DISCUSSION	
5.1	Characterization of the Silver Nanoparticles	
5.1.1	Determining Particle Size and Distribution	36
5.2	Membrane Functionalization with Silver Nanoparticles	36
5.3	Characterization and Morphology of the CA and Modified Membranes	
5.3.1	Polymerization of GMA	38
5.3.2	Verification of Membrane Functionalization.....	39
5.3.3	Membrane Morphology and Structure.....	41
5.3.4	Hydrophilicity of the Membranes.....	44
5.4	Filtration Experiments	
5.4.1	Flux Decline.....	45
5.4.2	Salt Rejection.....	47
5.4.3	Silver Leaching Crossflow Studies.....	47
5.5	Biofouling Studies	
5.5.1	Biofouling Experiments.....	49
6	CONCLUSIONS AND RECOMMENDATIONS	
6.1	Conclusions.....	52
6.2	Recommendations.....	53
APPENDICES		
APPENDIX A:	List of Abbreviations.....	55
APPENDIX B:	Data	57
REFERENCES	65
VITA	73

LIST OF TABLES

Table 4.1: Major cations/anions compositions of synthetic brackish and seawater for comparison	32
Table 5.1: Corresponding functional groups and wavenumber for FTIR spectra .	39
Table 5.2: Atomic % of the reaction scheme to create ^C Ag-NP/CA membranes ..	41
Table 5.3: Flux values obtained from dead-end filtration.....	45
Table 5.4: Salt rejections of CA, ^P Ag-NP/CA and ^P Ag-NP/CA membranes	47
Table 5.5: Leached silver from ^P Ag-NP/CA and ^C Ag-NP/CA membranes over a week	48
Table B.1: Flux data for CA membranes with DI water, and 10 ⁴ CFU/mL / brackish water	57
Table B.2: Flux data for CA membranes with DI water, and 10 ⁴ CFU/mL / brackish water	57
Table B.3: Flux data for CA membranes with DI water, and 10 ⁴ CFU/mL / brackish water	58
Table B.4: Flux data for ^P Ag-NP/CA membranes with DI water, and 10 ⁴ CFU/mL / brackish water.....	58
Table B.5: Flux data for ^P Ag-NP/CA membranes with DI water, and 10 ⁴ CFU/mL / brackish water.....	59
Table B.6: Flux data for ^P Ag-NP/CA membranes with DI water, and 10 ⁴ CFU/mL / brackish water.....	59
Table B.7: Flux data for ^P Ag-NP/CA membranes with DI water, and 10 ⁴ CFU/mL / brackish water.....	60
Table B.8: Flux data for ^C Ag-NP/CA membranes with DI water, and 10 ⁴ CFU/mL / brackish water.....	60
Table B.9: Flux data for ^C Ag-NP/CA membranes with DI water, and 10 ⁴ CFU/mL / brackish water.....	61
Table B.10: Flux data for ^C Ag-NP/CA membranes with DI water, and 10 ⁴ CFU/mL / brackish water.....	61
Table B.11 Salt rejection data from CA, ^P Ag-NP/CA and ^C Ag-NP/CA	

membranes	62
Table B.12: Crossflow silver leaching study for ^P Ag-NP/CA membrane	62
Table B.13: Crossflow silver leaching study for ^P Ag-NP/CA membrane	62
Table B.14: Crossflow silver leaching study for ^P Ag-NP/CA membrane	63
Table B.15: Crossflow silver leaching study for ^C Ag-NP/CA membrane	63
Table B.16: Crossflow silver leaching study for ^C Ag-NP/CA membrane	63
Table B.17: Crossflow silver leaching study for ^C Ag-NP/CA membrane	64
Table B.18: XPS At.% of three ^C Ag-NP/CA membrane performed in separate reactions	64

LIST OF FIGURES

Figure 1.1: Global Water Stress Indicator (WSI) in major basins.....	1
Figure 2.1: Pressure-driven membrane process.....	5
Figure 2.2: Range of applications for different membranes processes.....	7
Figure 2.3a-b: Schematic of (a) dead-end filtration and (b) cross-flow filtration ...	8
Figure 2.4: Depiction of immersion phase inversion where J_2 is solvent flux and J_1 is non-solvent flux.....	8
Figure 2.5: Spectra of top: <i>Nocardia</i> strain, middle: fouled layer of <i>Nocardia</i> , bottom: PSf membrane	12
Figure 2.6: FTIR spectra of membranes operated using virgin and copper charged PP feed spaces where in descending order, represents unfouled, 4, 24 and 48 hours biofouling filtration.....	13
Figure 2.7: Disinfection performance comparison between Ag-NPs (70.37% w/w Ag ⁰) encased in varying stabilizers: casein, dextrin (average molecular weight: 1670 g/mol) and polyvinylpyrrolidone (average molecular weight: 29,000 g/mol).....	18
Figure 2.8: Attachment of poly-GMA with primary amine via S _N 2 reaction.....	20
Figure 4.1: Glycidyl methacrylate polymerization reaction scheme	24
Figure 4.2: Experimental setup of mono-GMA polymerization reaction.....	25
Figure 4.3: Drying crushed polymerized GMA product over a week	25
Figure 4.4: Fabrication of a membrane through phase-inversion process.....	26
Figure 4.5: Fabrication of CA/GMA membranes.....	27
Figure 4.6: Fabrication of chemically attached Ag-NP/CA membranes	28
Figure 4.7: Dead-end filtration schematic	31
Figure 4.8: Crossflow filtration parts and schematics	33
Figure 5.1: (a) TEM images of dried casein-coated Ag-NPs and (b) particle size distribution.....	36
Figure 5.2: Proposed reaction of CA with GMA to form CA/GMA membranes..	37
Figure 5.3: Fabrication of ^C Ag-NP/CA membranes	38
Figure 5.4: Progression of the GMA polymerization reaction	39

Figure 5.5: XPS spectra (150-550 eV) of CA, CA/GMA, CA/GMA/CYS and CA/GMA/CYS/Ag-NPs membranes with corresponding core level peaks.....	40
Figure 5.6: Cross section SEM images of (a) 18%CA, (b) ^P Ag-NP/CA and (c) ^C Ag-NP/CA membranes	41
Figure 5.7: SEM imaging of (a) 18%CA, (b) ^P Ag-NP/CA and (c) ^C Ag-NP/CA membranes pores	42
Figure 5.8: EDX mapping analysis of ^P Ag-NP/CA membranes.....	43
Figure 5.9: EDX mapping analysis of ^C Ag-NP/CA membranes	44
Figure 5.10: Contact angles of virgin and modified CA membranes	44
Figures 5.11: Filtration of CA, ^C Ag-NP/CA and ^P Ag-NP/CA membranes all performed at 4.14 bars (60 psi).....	47
Figure 5.12: Fluorescence microscopy images of live/dead cells detached from (a-b) CA, (c-d) ^P Ag-NP/CA, and (e-f) ^C Ag-NP/CA membranes respectively (All images were brightened to create better contrast of the images for easier observation).	50

1 INTRODUCTION

The most basic and essential resource for life is water [1]. Unfortunately, the increase in global population has led to a severe shortage of readily accessible clean water. Several regions of the world are faced with increased stress index of water use and are likely to increase along with population growth, *Fig. 1.1* [2]. Lack of water affects one in three people globally, with 25% of people worldwide living in locations where water is physically or economically scarce [3]. According to the World Health Organization (WHO), in 2008, 13% world population (approximately 884 million people) lived with little to no access to sufficiently clean water sources [4]. Drought, desertification, and agricultural, industrial and domestic uses are all rapidly contributing to the decrease of fresh water sources [5]. The remaining available water is insufficient to meet societal needs [3]. Therefore, developing solutions to provide clean water from impure sources, such as sea, brackish and wastewater, becomes paramount. Treating impure water sources to produce clean drinking water might be possible via membrane separations.

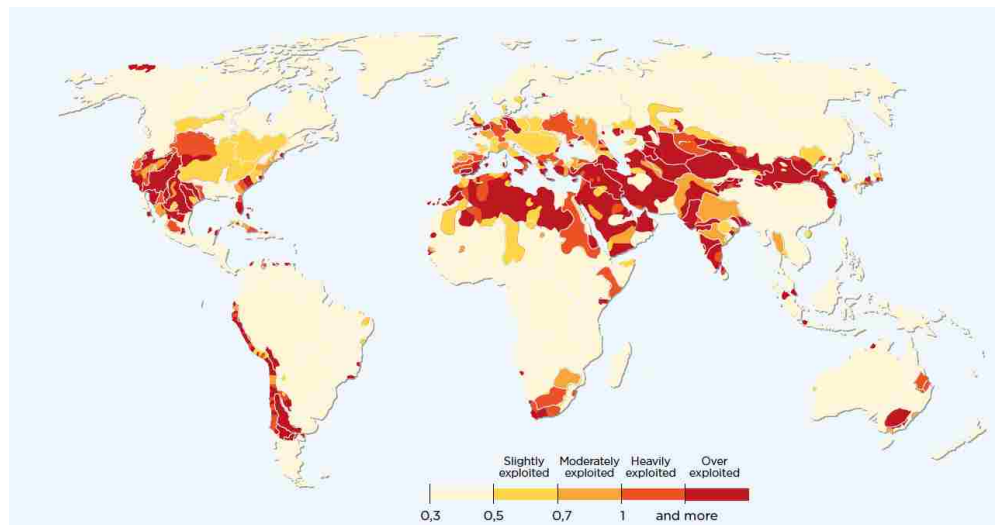


Figure 1.1 Global Water Stress Indicator (WSI) in major basins [2]

Membranes can produce high-quality drinking water from fresh, brackish, seawater and water reuse sources [3]. Common membranes processes include microfiltration (MF), ultrafiltration (UF), nanofiltration (NF) and reverse osmosis (RO) [3, 6]. Although membranes are effective for water purification, they are susceptible to

impaired efficiency due to fouling, which is the accumulation of rejected materials remaining on membranes following water purification, such as particles, macromolecules, colloids, salt, etc. [7, 8]. There are four different types of fouling: *organic fouling* (adsorption of organic matter), *scaling* (salt precipitation or surface nucleation), *biological fouling* (mainly from biofilm development) [9], and *colloidal fouling* (particle buildup) [8].

Membranes are made from many types of polymers, such as polyacrylonitrile (PAN), polyamide (PA), polyimide (PI), poly(tetrafluoroethylene) (PTFE), poly(vinylidene fluoride) (PVDF), polysulfone (PSf), polyethersulfone (PES), cellulose, etc.[10]. Cellulose acetate (CA) in particular is inexpensive, hydrophilic, resistant to chlorine, and has low susceptibility to fouling [11]. Its negative surface charge can provide charge repulsion between the membrane surface and bacteria to provide some biofouling control. However, CA can be readily biodegraded by organisms that reach its surface and utilize cellulase enzymes [12]. Therefore, it is important to provide CA with additional antimicrobial properties, and one method of doing such is by the incorporation of biocidal metals [13].

The objective of this study was to control membrane biofouling in CA membranes to be used as potential pretreatment options for more retentive processes, such as RO and NF. Biofouling results from the growth of microorganisms present on membrane surface [8, 14] that produce a biofilm. Many strains of bacteria, such as *Staphylococcus*, *Salmonella*, *Enterococcus* and *Pseudomonas*, produce extracellular polymeric substances (EPS), which create a tough matrix on the membrane surface and may lead to membrane biodegradation, clogging of pores, higher operating costs, increased pressure drop, and other performance issues [14-16]. Biofilms continue to grow at the expense of available nutrients in the feed water and create microbial aggregates that adhere to membrane surfaces [15, 17]. It is extremely difficult to completely eradicate biofouling. Even if 99.9-99.99% of all bacteria are removed from the membranes, the remaining cells can become entangled into the system, remain protected, attach to the surface, start to colonize and multiply at the expense of available nutrients [17-19].

In order to control membrane biofouling, feed waters can be pretreated [20], particles can be removed [21], the membrane can be cleaned via backwash (or reverse

flow) and/or chemical treatment, or membranes can be modified to create antifouling materials via graft polymerization, UV irradiation and other processes [22]. Pretreatment allows the efficiency and life expectancy of membranes to be maintained through removal of foulants before these reach the main process membranes [23]. Processes such as UF and MF are predominantly used as pretreatment options to remove larger particulates and microorganisms before more retentive processes (NF and RO) are used [3, 24], which helps reduce the need of chemicals [14]. For pretreatment, disinfectants (such as chlorine) may be used to control biofouling to boost membrane's life expectancy, but many membranes cannot withstand the corrosiveness of chlorine [20]. Thus, pretreatment can be performed with other disinfectants, such as ozone and potassium ferrate [19] to maintain membrane durability [25]. Polymers such as cellulose acetate and polyamide possess considerable resistant to chlorine, but are limited by operational pH ranges, salinities, molecular state, etc. [26]. Functionalizing membranes with desirable properties, such as hydrophilicity and charge, can be performed using several different methods, such as surface coating and grafting [27]. Of focus here is the incorporation of nanoparticles on the membrane [22].

Silver nanoparticles are chemically stable, possess catalytic and conductive properties, and are more antimicrobial than other metals [28-30]. Three possible mechanisms for silver's antimicrobial properties include: damage of microbial cell membranes and intracellular components (through interaction with protein thiol groups and inactivation of enzymes), adsorption onto microbial cell walls, and creation of reactive oxidative species (ROS) [20, 22, 31]. In addition, gram-negative bacteria possess negatively charged lipopolysaccharide surfaces, which create electrostatic attractions between the silver and bacteria. Ag-NPs have sizes less than 100 nm, while silver ions are in ionic form, commonly oxidized from metallic silver [32]. Smaller nanoparticles have enhanced surface-to-volume ratio that allow for more interaction sites between ions and bacteria [7, 33]. Ag-NPs photocatalytic and surface properties are favorable towards biocidal activities and are much more toxic than Ag⁺ ions [32].

However, nanoparticles tend to agglomerate, due to steric repulsion effect, attraction interaction, and the presence of ions and natural organic matter (NOM) [34]. Agglomerating NPs leads to fewer surface area interactions available, which decreases

their antimicrobial properties [7, 33, 35-37]. To minimize agglomeration, compounds, such as dextrin (made from maize starch), polyvinylpyrrolidone (PVP), or casein can be used to encapsulate nanoparticles [34]. Studies have shown that these encapsulating agents have similar properties and performances, but their stabilities with Ag-NPs can be different based on the binding forces [34]. It was suggested that casein had stronger binding forces over PVP and dextrin due to its complex steric configurations and electrostatic properties, which led to better stability effects for encapsulation [38]. Casein possesses excellent biocompatibility and biodegradability, pH-responsive functionality and is stable up to 60-70°C [39].

Studies using nanocomposite membranes have shown that silver nanoparticles may leach from membranes [8, 20, 40], which decreases antimicrobial performance. Furthermore, the presence of leached silver in water violates secondary maximum contaminant levels (SMCL) for silver ions (0.1mg/L or 100 ppb [41]). To address silver leaching, Ag-NPs have been immobilized onto membranes through interactions between carbamate groups on polyurethane foams [42], irradiation (wavelength of 245 nm) onto electrospun CA nanofibers [36], cysteine groups on PA/TFC composite membranes [43], among others.

The overarching goal of the research thesis was to functionalize CA membranes with Ag-NPs to produce low-biofouling membranes for potential pretreatment processes. Immobilizing Ag-NPs on membranes reduces the amount of leaching; however, it also decreases the available interaction sites to potentially decrease their antimicrobial function. Therefore, an immobilization technique was sought that would simultaneously prevent silver nanoparticle leaching while maintaining its antimicrobial function. The functionalization of Ag-NPs onto the CA was achieved via attachment with functionalized thiol groups. Thiol groups were chosen as an attempt to imitate the biocidal nature of Ag⁺ where they attach to thiol groups that make up many bacterial structures, such as proteins that contain cysteine [20, 22, 31].

2 LITERATURE REVIEW

2.1 Membranes

2.1.1 Membrane Separation Mechanisms

A membrane acts as a selective barrier which regulates the transport of substances between two adjoining phases [44]. Membrane processes are potentially sustainable processes that can provide efficiently high-quality water from fresh, brackish, seawater and wastewater sources [3]. Membranes are typically composed of two layers: a porous support and a thin selective film. The support layer provides mechanical strength and stability, while the latter is responsible for the membrane selectivity and properties [45]. *Fig. 2.1* illustrates a pressure-driven membrane separation system where a solution is being passed through a semi-permeable membrane. A pressure difference between the feed and permeate sides facilitates the movement of solutions through the membrane during the separation process [6]. The concentrated solution that is retained by the membrane is known as the *retentate* or concentrate or brine, whereas the *permeate* is the dilute solution that passes through the membrane [46]. The driving force of the system can be influenced by changes in chemical potential gradient (i.e., concentration and pressure [44]), electrical voltage and temperature [46].

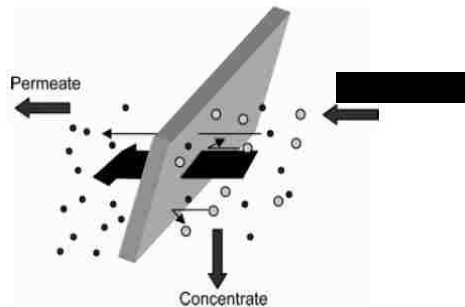


Figure 2.1: Pressure-driven membrane process [45]

The amount of feed that flows per square unit area is defined as flux, which is represented as J ($L/m^2 \cdot h$) [46, 47]. Flux due to diffusion can be described by Fick's first law:

$$J_i = -D_i \frac{\partial c_i}{\partial x}$$

where J_i represents the flux component of the species, D_i is the diffusivity of the species, and $\partial c_i / \partial x$ represents the concentration gradient of species i . Flux is dependent on the concentration gradient, and the negative sign shows that the gradient proceeds in the negative direction where it flows from high to low concentration regions.

Membrane processes are divided based on their pore sizes: microfiltration (MF), ultrafiltration (UF), nanofiltration (NF) and reverse osmosis (RO) [48], as shown in *Fig. 2.2*. RO and NF are diffusion-controlled membrane processes [6, 48], but NF also allows pore flow due to its relative pore size of 1-5 nm and charge repulsion effects [48, 49]. RO does not necessarily have distinct pore sizes and is termed nonporous, because RO membranes are often web-like with thick, twisting pathways towards the permeate side of the membrane [50]. RO requires significantly higher pressure gradients for flow, because its operation is based on the diffusion of ions and salts against the concentration gradient [50]. Both RO and NF processes are able to retain most organic and inorganic substances, along with microorganisms from raw water sources, to produce clean water [51]. They require high operating pressures: 20-100 bars for RO and 7-30 bars for NF [46, 48]. NF is able to retain divalent ions, and is often used for water softening (or the removal of calcium and magnesium), at a higher rate than monovalent ions [52], along with organics with low molecular weights [48, 49]. Due to the ability of RO to retain salt and ions, RO is mainly used for desalination [3, 53]. While both processes are not commonly used for disinfection, the two processes can retain viruses and bacteria [14]. The effectiveness of the processes depends on the membrane properties, hydrodynamics feed water composition, and any potential interactions between the three [51]. However, both NF and RO processes deteriorate from concentrate treatment and disposal requirements [14, 54, 55].

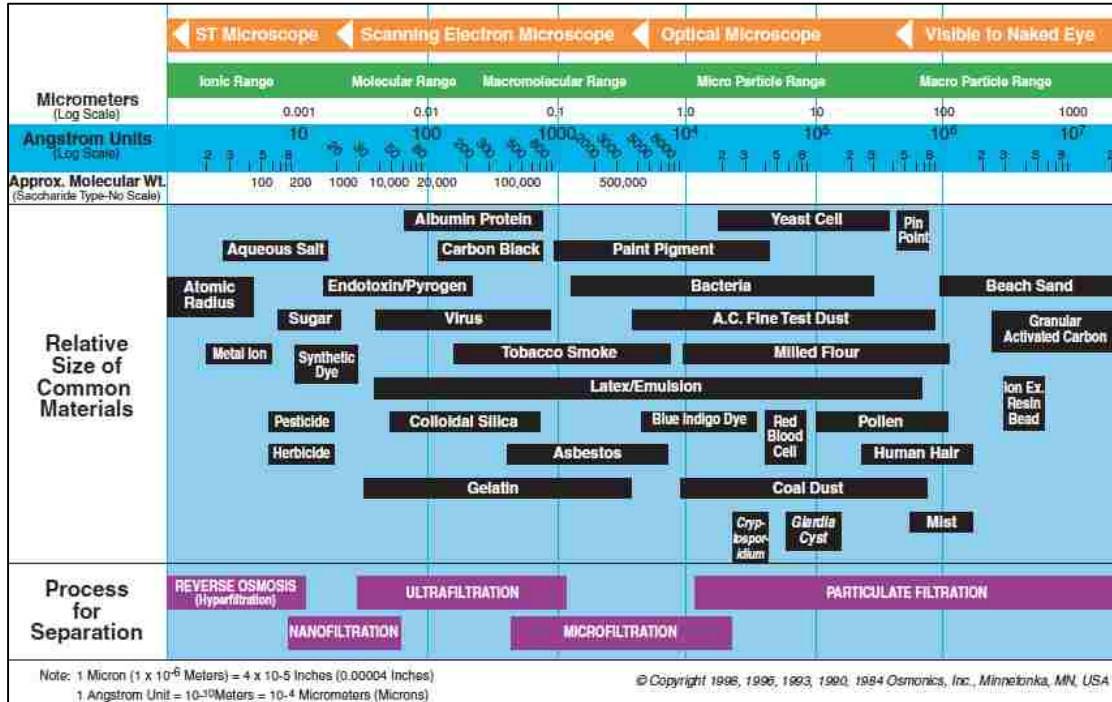


Figure 2.2: Range of applications for different membrane processes [56]

The separation processes of MF and UF are controlled by the size exclusion principle [44], where larger molecules are retained and smaller ones pass through. UF membranes typically have pore sizes of about 5-20 nm, while MF membranes have pore sizes of 50-1000 nm [46]. UF and MF membranes require smaller operating pressures of 1-10 bars and 0.1 bars, respectively [46]. UF retains macromolecules, colloidal, and microorganisms [48, 52], and is able to reject viruses, bacteria, and organic matter [57]. Larger molecules, such as dissolved organic carbons, are often not retained by MF because the pore sizes are too large to retain these substances [24]. UF and MF are popular among water pretreatment technologies for hybrid membrane applications. They are predominantly used to remove larger particulates and/or suspended microorganisms before more retentive processes, such as NF and RO, are implemented [3, 24], because they can be configured to provide higher levels of pathogenic removal without chemical addition [14].

Two typical types of configurations are used to operate membrane processes: dead-end and cross-flow filtration. In the case of dead-end filtration, all feed solution passes through the membrane, and any colloids larger than membrane pores build up and settle on the surface, *Fig. 2.3*. With cross-flow filtration, the feed solution passes parallel

to the surface of the membrane with the pressure driving force being applied perpendicular. While this configuration minimizes the buildup of rejected materials on the surface, a fraction of the feed solution becomes retentate [58].

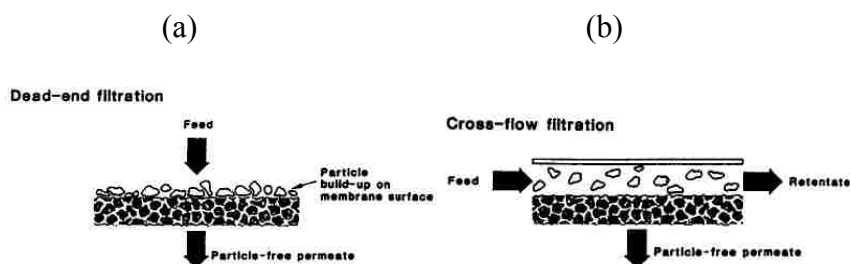


Figure 2.3: Schematic of (a) dead-end filtration and (b) cross-flow filtration [58]

2.1.2 Membrane Formation

Membranes are synthesized from dope solutions, which are composed of a polymer, a solvent and any necessary additives, such as pore formers. They can be fabricated using different methods, such as phase inversion, dip-coating, track-etching, sintering, etc. [10, 59]. Of interest here is phase inversion, which is arguably the most common method of casting polymeric membranes. It was first performed with porous nitrocellulose papers in 1907 [60], and helped influence the development of the Millipore Corporation and Amicon Corporation in the later years [60]. In phase inversion, a soluble solution is converted into a solid form. The method involves a dope solution, which is cast on a substrate and later submerged in a non-solvent coagulant bath, usually water. In the water bath, the polymer eventually becomes supersaturated with the non-solvent (water) through a process known as immersion precipitation, where the polymer changes from a solution state into a solid state, thus creating a membrane, *Fig. 2.4* [60].

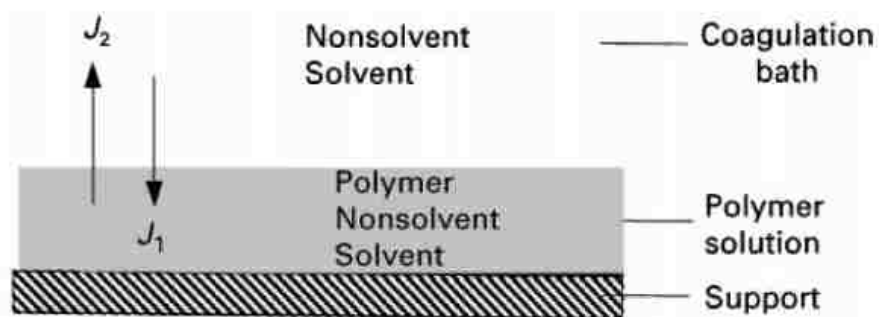


Figure 2.4: Depiction of immersion phase inversion where J_2 is solvent flux and J_1 is non-solvent flux [60]

The rate of evaporation is dependent on the solvent, non-solvent, temperature, polymer, etc. The process of liquid-liquid demixing plays the main role in phase inversion, which helps explain the formation mechanisms of the membranes [59]. When a polymer and solvent are initially mixed together, they are considered to be thermodynamically stable. When the exchange of solvent and non-solvent has proceeded beyond a certain point, the solution reaches its thermodynamically unstable state, and demixing occurs [60], which can be affected by concentration of solvent and polymer, solvent bath, temperature and time. The time it takes for the demixing process to occur is an important factor in governing the membrane morphologies [59]. For example, under fast demixing conditions, membranes are expected to have a thin top layer and sublayer filled with macrovoids [60]. The top layer is expected to be porous and have nodular structures present [59]. Slow demixing conditions facilitate the production of thick dense top layers, which results in low porosity and permeability due to high concentration of polymer from the beginning of demixing [59].

Many factors influence membrane casting via phase inversion, such as room humidity, water temperature, viscosity of the dope solution, choice of solvent, polymer concentration, thickness gauge, evaporation period, air bubbles, and other factors. Thickness and polymer concentration affects pore size and performance. Polymer concentration affects dope viscosity, which impacts the diffusion delay of non-solvent (water) through the phase-inversion process, which in turn decreases coagulation rates [30]. Temperature controls the demixing process and affects the morphology of the membranes based on the solvent and polymer [59].

2.1.3 Membrane Materials

Choice of polymer affects membrane characteristics and properties, such as charge, adsorptivity, stability, and hydrophilicity for porous membranes [10]. For nonporous membranes (such as RO), solubility and diffusivity also depend on the chemical structure of the membranes [10]. There are a wide variety of polymers commonly used for porous membranes: such as cellulose acetate (CA), acrylic, polysulfone (PSf) and other patented noncellulosic polymers [52]. Porous membranes

had also been prepared with polycarbonate (PC), polyvinyl chloride (PVC), poly(vinylidene fluoride) (PVDF), polyamide (PA), polyacrylates, etc. [52].

Cellulose acetate (CA) is a commonly used membrane material since it is inexpensive, and possesses good hydrophilicity, chemical resistance and low overall susceptibility to fouling; however, CA is biodegradable and only suitable for operation in the pH range of 2-8 [3, 9, 11, 15, 49, 61, 62]. It also suffers from low mechanical strength and low thermal resistance [11]. CA is formed from the esterification of acetic acid and cellulose. CA membranes are asymmetric, meaning they are composed of a dense top layer and porous sublayer, and can be used for many different applications including UF, RO, gas separation, and blood dialysis [25, 61]. However, studies have shown that these membranes succumb to low permeability and poor solute selectivity [49]. CA membranes have relative high tolerance to free chlorine (up to 5 ppm), but are susceptible to hydrolysis and begin to degrade at temperatures higher than 35°C [3, 15, 52, 62]. CA's high hydrophilicity is due to the acetyl groups, and CA membranes possess an isoelectric point of 3.5, which suggests a negative surface charge [63]. It is studied that CA acetyl's content is proportional to salt rejection and inversely proportional to water flux [52]. Many problems associated with CA membranes occur from the hydrolyzing properties due to sudden changes in the pH. Cell adhesion on CA membranes is independent of pH changes [64], and the negative surface charges on CA membranes helps with biofouling control because bacteria surfaces often possess negative charges; hence creating repulsive forces between the two surfaces [65]. CA can be readily biodegraded by organisms that reach its surface and utilize cellulase enzymes [12]; therefore, controlling biofouling is critical for CA membranes.

2.2 Fouling

2.2.1 Types of Fouling

Four different processes are associated with fouling: *organic fouling* (adsorption of organic matter), *scaling* (salt precipitation or surface nucleation), *biological fouling* (mainly from biofilm development) [9] and *colloidal fouling* (particle buildup) [8]. Natural organic matter (NOM) primarily causes organic fouling [66] and accumulates on the membrane surface and pore structure [67]. Organic matter fouling is often associated

with microbial cells debris adsorption and suspension on membrane surfaces [19]. In addition, any particles present on the membranes can interact with NOM, which influences side interactions/reactions to create more fouling problems [66].

Scaling occurs when dissolved salts and mineral concentration is beyond the solubility limit of the solution, which can lead to pore clogging, pore wetting [3] and cake formation [66]. Major ions that induce scaling include magnesium, barium, calcium, bicarbonate and sulfate [68], because they can form into insoluble salts and accumulate on the membranes [67].

Colloidal fouling, caused by large organic macromolecules, suspended matter, clays [69] and biological contaminants [70], is considered to be the main cause of membrane fouling [69]. Unwanted interactions with the membranes can lead to reduced membrane performance from buildup, failure and/or increased wettability of the membranes [44]. Most colloids tend to form a cake/gel layer on membrane surfaces [19], where interfacial tension forces can trap them on the membrane-liquid interface of the surface [3].

Lastly, biofouling results from the accumulation of live/dead microorganisms present in water on the membranes. Over time, this phenomenon can lead to biofilm formation and cause major performance problems to water treatment systems, such as clogging of pores, higher operating cost, higher pressure drop, etc. Several factors influence biofilm development, including temperature, pH and redox potential [18, 71]. Biofilms excrete extracellular polymeric substances (EPS), composed mainly of polysaccharides and proteins, but also contain heteropolysaccharides, lipoproteins, glycolproteins, and other large macromolecule sources [72, 73]. EPS formation allows microorganisms to grow more readily because it creates regions where bacteria can attach and grow protected.

Completely preventing the growth of biofilm is exceedingly difficult. Even if 99.9-99.99% of all bacteria are destroyed, any remaining cells can become entangled into the system, remain protected, attach to the surface, start to colonize and multiply at the expense of nutrients available [18]. Changes in nutrients, external stresses, temperature, pH, etc. can alter biofilm formation [18, 74]. Biofilms act as a mean of self-defense, create favorable niches, and provide conditions for close bacterial interaction [65]. Such

niches allow bacteria to grow more closely to each other and allow more chances of nutrient and genetic exchange, leading to other possible mutations [65]. A noticeable change in pressure or flux is usually an indication of biofouling. Spectroscopical analysis, such as Fourier transform infrared spectroscopy (FTIR), is commonly used for the detection of EPS, in particular the polysaccharide peaks [8, 17]. It is possible to pick up indication of biofouling from investigating the polysaccharide bands emitted from the EPS on the membrane surface [8, 17]. An example of distinguishing such peaks can be found in *Fig. 2.5*, where the *Nocardia* spectrum (middle) is shown to be distinguishable and its unique lipids and polysaccharides shows the membrane is fouled [73].

Another example of the use of FTIR in the detection of biofouling is shown in *Fig. 2.6*, where Hausman et al. provided a comparison between operating NF polyamide membranes using virgin polypropylene (PP) feed spacers and copper-charged ones through a series of biofouling filtration experiments of varying durations. There were less noticeable signs of biofouling on the membranes that used feed spacers charged with copper. On the other hand, membranes that used virgin (or unmodified) feed spacers showed biofouling peaks at $900\text{-}1200\text{cm}^{-1}$, 1400cm^{-1} and 1468cm^{-1} . These represent polysaccharides, amino acids; fatty acid chains and lipids/lipopolysaccharide, respectively [17], which are main components of biofilms.

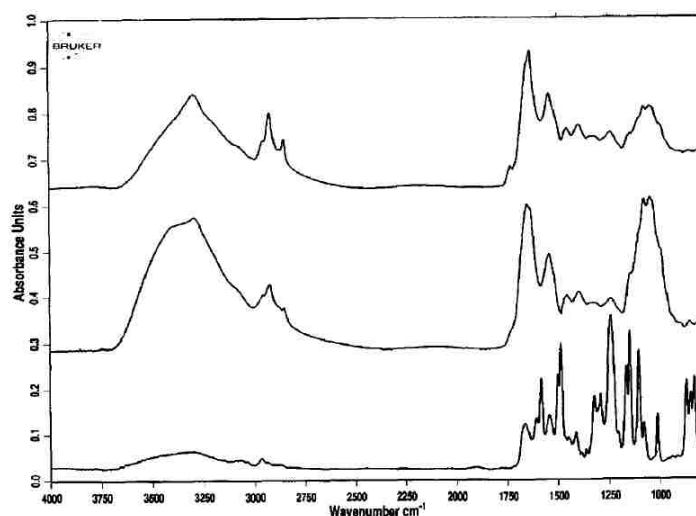


Figure 2.5: Spectra of top: Nocardia strain, middle: fouled layer of Nocardia, bottom: PSf membrane [73]

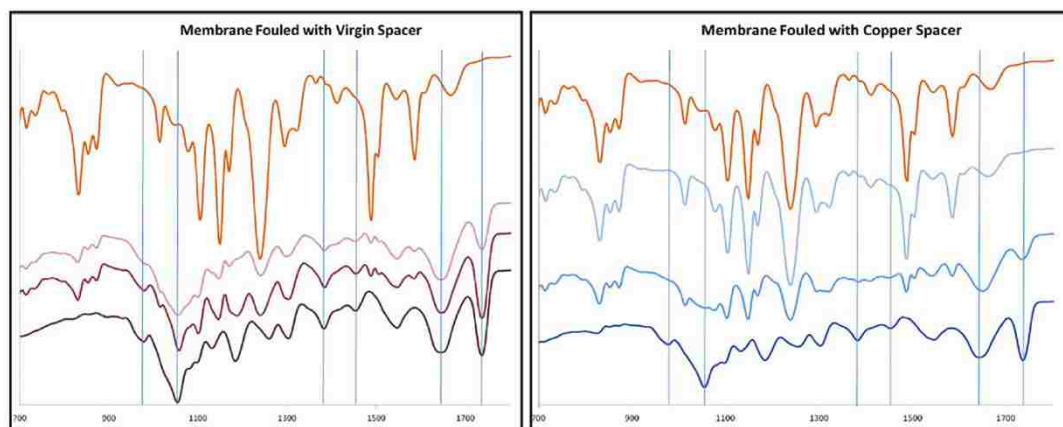


Figure 2.6: FTIR spectra of membranes operated using virgin and copper charged PP feed spacers where in descending order, represents unfouled, 4, 24 and 48 hours biofouling filtration [17]

2.2.2 Fouling Control

The predominant forces contributing to attachment of foulants are due to dispersion and polar interaction forces [67]. The dispersion interaction forces are controlled through Van der Waals attraction forces and can be controlled through maintaining electrostatic repulsion of the foulants and membrane [67]. Polar interaction forces are controlled through Lewis acid/base pairs that may be present in the system. This helps explain the common need of increasing membrane hydrophilicity to reduce attachment of foulants [67].

Growth of bacteria is based on temperature, water flow, pH, and the availability of nutrients [75]. Microbial growth can be promoted by any source of nutrients, even inorganic for lithotrophic organisms [18]. Furthermore, bacteria preferentially grow attached to surfaces in aqueous environments, rather than be free floating [75] since surfaces provide protection for bacteria through the development of a biofilm. Microbial activity increases in rougher surfaces over smooth surfaces [18], because small crevices allow more places for bacteria to thrive due to less exposure to moving water. Rougher surfaces contain more surface area, where the ridge-ness of the surfaces is more favorable for foulants accumulation through more adsorption sites [66, 69]. However, rougher surfaces often provide more area for flow and are a desirable characteristic with respect to encouraging microbial growth.

Taking steps to minimize biofilm formation is more realistic than trying to eradicate microorganisms, such as through chlorination, yet only a few methods exist to prevent biofilm formation without compromising membrane function. Fluid velocity of water greater than 1 m/s has been shown to help impede biofilm formation [75], yet higher velocities can create biofilms that are more dense and compact [76, 77]. Melo et al. explained that an increase of velocity from 0.13 m/s to 0.54 m/s resulted in biofilm formation thickness from 26 kg/m³ to 76 kg/m³ using *Pseudomonas fluorescens* [75]. Other factors, such as availability of nutrients, presence of disinfectants, bacteria and piping materials, can influence larger biofilm formation when higher velocity flows are used [77]. Cells adhesion to surfaces to form biofilms is governed by electro-kinetics, hydrophobic interactions [72], surface roughness and materials used [19]. In order to break up interactions between adhering cells and surfaces, the bonding energy must be overcome, which is 0.1-10% of carbon-carbon bonds based on the presence of macromolecules, the pH of the solution, the ionic strength, etc. [73].

Since UF is associated with many forms of fouling, several methods have been taken to control it through ultrasonication, membrane surface modifications, backwashing, pre-treatment, etc. [30]. Sound waves created by ultrasonication lead to cavitation and acoustic streaming that cause vigorous mixing to occur, which in turn breaks up caked layers on membranes [19]. The cavitation facilitates detachment of foulants from the membrane, while the acoustic streaming facilitates foulants movement away from the membranes [19]. Rana et al. described a wide variety of methods to reduce fouling from increasing surface hydrophilicity through surface modifications [78]. Wenten et al. described a novel backwashing technique known as “backshock,” where using extremely short backflush time (0.06 seconds) for 1-3 second intervals resulted in prevention of pore blocking [53, 79]. The low backwash time coupled with high pressure caused negligible permeate loss.

Inactivation of DNA has been achieved through pre-treatment with UV irradiation at a wavelength of 254 nm [80], yet the process cannot control biofilm development [19]. The application of pre-treatment chemicals, such as sodium hypochlorite, are used intensively to chlorinate water and inactivate microorganisms, yet sodium hypochlorite reacts with humic substances in water to form harmful disinfection byproducts [25].

Application of chlorine works well against biofilm formation on CA membranes, yet the membranes cannot withstand extensive exposure to chloride ions, and the membranes ultimately degenerates over time [15]. Because of this, the use of other disinfectants, such as ozone, potassium ferrate [19], is considered more favorable towards membrane durability [25]. The weak electrostatic interaction of biofilm formation can be interrupted by the addition of cleaning agents, such as citric acid, salts, phosphates, complex formers, etc.; yet this does not work for all strains, such as *P. diminuta* on PSf membrane surfaces [73].

To prevent biofouling, membranes and membrane systems have also been functionalized with biocidal metal ions. For example, Hausman et al. functionalized PP feed spacers with metal chelating ligands to develop low-biofouling membranes [8]. They investigated the use of silver and copper ions and concluded that the incorporation of these ions improved the membrane performance by decreasing cell adhesion to membrane surfaces [8]. In other studies, chitosan was introduced into films to increase hydrophilicity and provide the membranes with antimicrobial properties; however, performance decreased due to water moisture and acids (such as acetic acid, citric acid and weak HCl) [81].

2.3 Silver Nanoparticles

2.3.1 Properties of Silver Nanoparticles

Silver nanoparticles (Ag-NPs) have antimicrobial properties due to their small size, large surface area and their ability to become lodged into matrixes [13]. Nanoparticles (NPs) are more favorable over microparticles, due to an almost 1000-fold increase in surface area per unit weight, which allows more chemical interactions [33, 35]. Nanoparticle properties are dependent on size, extent of dispersion, and structure [36]; however, nanoparticle agglomeration leads to reduced cell-particle interaction, membrane penetration and the release of silver ions [33], so stabilization through capping is often needed. With enhanced surface-to-volume ratio, there are more potential interaction between ions and bacteria [7, 33]. Several types of NPs, such as zinc, titanium, magnesium, copper, alginate and gold, have been used for antimicrobial use,

but silver remains the most effective against viruses, bacteria and other eukaryotic microorganisms [82].

Silver is bacteriostatic [83], so cells become deactivated but not necessarily killed. There are three possible mechanism for silver's antimicrobial properties: damage of microbial cell membranes and intracellular components, adsorption onto microbial cell walls, and creation of reactive oxidative species (ROS) [33]. Choi and Hu demonstrated that Ag-NPs smaller than 5 nm expressed more toxicity towards cells internally, possibly due to easier transport of uncharged Ag-NPs across cell membranes [84]. These smaller Ag-NPs entering cells were able to disrupt cellular replication and inactivate vital enzymes [85]. In addition, Ag-NPs small sizes could encase the cell membrane surface, which resulted in reduced proliferation of cells [86]. *Pseudomonas*, *Staphylococcus epidermidis*, *Escherichia coli*, methicillin-resistant *S. aureus* (MRSA) and methicillin-resistant *S. epidermidis* (MRSE) have been shown to be vulnerable to Ag-NPs [25]. *Pseudomonas fluorescens* are gram-negative rod-shaped bacteria [87]. Since these bacteria are gram-negative, it was suggested that Ag-NPs are more attracted to them [35] due to the negatively charged lipopolysaccharide (LPS) layers present on the bacterium surfaces, which create attraction forces between the Ag-NP's positively charged particles.

ROS are able to increase the rate at which cells are programmed to die through disruption of the aerobic respiration process by producing reduced forms of oxygen [13]. In the presence of metals, electrons can be stripped from other forms of oxygen molecules (donors) and increase the present of ROS derivatives [13]. Overall, an oxidative stress is created on the cells [13]. Hydroxyl radicals (OH[·]), produced from oxidizing hydrogen peroxide (H₂O₂), are extremely powerful oxidizing radicals and can react with nearly all biomolecules [88]. Biomolecules stripped of their hydrogens create oxidative damage of the cell, and shortened life span [13]. Ag⁺ ions can oxidize fatty acids double bonds and result in greater permeability which leads to greater osmotic stress [35].

Studies have shown that Ag-NPs can attach to the thiol groups of bacterial cysteine groups, which leads to inactivation of enzyme and replication [35, 37, 85]. If bacterial cell walls contain proteins with -SH groups, the cell walls are prone to have their functionality compromised due to Ag⁺ interactions [86]. Cysteine can render Ag⁺

ions unavailable by forming complexes with silver released from the NPs [20, 32]. This lowers the antimicrobial aspects of the Ag-NPs in the first place because of the formation of complexes. Key factors controlling Ag-NP antimicrobial activity include size, shape, zeta potential, pH, etc. [20, 33, 35, 37]. Furthermore, metallic Ag-NPs can be oxidized in the presence of moisture, which facilitates silver ion leaching from surfaces to decrease the surface antimicrobial properties [37].

2.3.2 Silver Nanoparticle Stabilizers

In order to control the agglomeration and dispersion of NPs, capping agents and ionic strength control are usually employed [37]. Many synthetic and natural polymers have been incorporated as Ag-NPs stabilizers, including polyvinylpyrrolidone (PVP), polyvinyl alcohol (PVA), polyacrylates, polyacrylamide [37], dextrin and casein [34]. Of interest, casein is a milk protein that possesses excellent biocompatibility, biodegradability, pH-responsive functionality and is stable up to 60-70°C [39]. Zhang et al. proposed that casein and Ag-NPs bound together through the complexation of the carboxylate or amino group [33]. While the exact casein structure is unknown, its complex steric configurations and electrostatic properties likely contribute to its stabilizing effects [34]. Its ability to change configuration and properties when induced by different environmental conditions makes casein more susceptible to binding onto ions [39]. *Fig. 2.7* shows the disinfection performance of three different stabilizers encapsulating Ag-NPs. There were no statistically significant differences between the disinfection performances observed for the different capping agents under different waters. Therefore, casein was found to be a viable capping agent for silver nanoparticles.

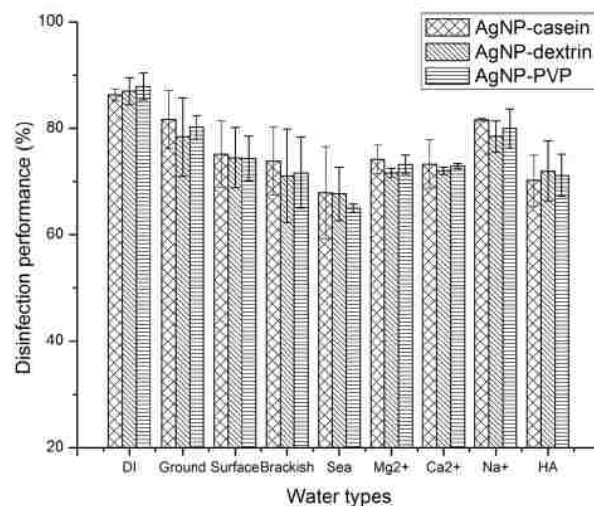


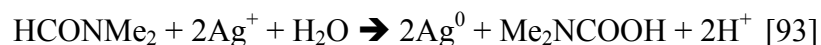
Figure 2.7: Disinfection performance comparison between Ag-NPs (70.37% w/w Ag⁰) encased in varying stabilizers: casein, dextrin (average molecular weight: 1670 g/mol) and polyvinylpyrrolidone (average molecular weight: 29,000 g/mol) [34]

Additional inferences about the effects of different water types on the disinfection performance of Ag-NPs are also shown in *Fig. 2.7*. Natural water sources (surface and brackish water) showed similar performances, which was hypothesized to be due to NOM adsorption on Ag-NPs. This could create physical barriers between the Ag-NPs and the cells and inhibit silver toxicity [34]. Likewise, a lower NOM content could account for the higher disinfection performance of groundwater [34]. The reduced performance observed with seawater was likely due to other anionic ligands, such as Cl⁻, precipitating silver into salts and inhibiting its toxicity [89]. Through the Schulze-Hardy rule, Zhang et al. found that Ag-NPs were sensitive to counter ions present in the solution, such as divalent cations, which promoted aggregation [34]. When silver agglomeration occurred, silver formed sediments and settled in solutions [37].

2.3.3 Chemical and Physical Functionalization of Silver Nanoparticles to Surfaces

Nanoparticles have been shown to not mix well with polymeric dope solutions leading to inconsistent mixing, increasing NP agglomeration, and decreasing membrane efficiency [90, 91]. Even through consistent sonication, agglomeration is difficult to prevent. Solvent use for the preparation of dope solutions can also be a factor. Using DMF solvent as a reducing agent to the silver with CA and 80°C heat has resulted in

dispersed films populated with Ag-NPs [81]. DMF is an effective reducing agent for converting Ag^+ ions into NPs [37, 81, 82, 92], according to the following reaction scheme



Ag-NPs were introduced on polysulfone (PSf) UF membranes by Zodrow et al. [20], CA hollow fiber membranes by Chou et al. [25], polyamide (PA) TFC membranes by Yang et al. [94], CA UF membranes by Asapu et al. [15], carbon nanofibers by Abdo et al. [82], polyacrylonitrile (PAN) membranes by Lee et al. [92] and many others. Immobilization of NPs is important, because over time they might leach from the membranes. Studies with reducing agents, such as Vitamin C [95] have been performed to immobilize these NPs. Prince et al. successfully immobilized Ag-NPs and polyethylene glycols (PEG) through the use of poly(acrylonitrile-comaleic acid) PANCMA onto polyethersulfone (PES) hollow fiber UF membranes [30]. Jain et al. showed that nitrogen atoms on polyurethane membranes could bind with the NPs through the $-\text{N}(\text{H})\text{COO}-$ (carbamate) groups [42]. The polyurethane (PU) foams were soaked in Ag-NPs solution, which led to complete surface coating of the membranes, where different exposure time affected the surface coverage. Son et al. developed a novel technique where Ag-NPs were irradiated onto electrospun CA nanofibers through ultraviolet radiation at a wavelength of 245 nm [36]. The nanofibers displayed high surface area and porosity, with more opportunities for Ag-NPs to be attached. Kwon et al. showed through infrared spectroscopy and ultraviolet spectroscopy, that about 95% of Ag-NPs had the potential to leach from CA at room temperature [96]. Yin et al. functionalized Ag-NPs through cysteine groups onto the surface of PA/TFC composite membranes [43]. In the study, the cysteine groups, $\text{NH}_2-(\text{CH}_2)_2-\text{SH}$, were attached to the TFC membrane, and the Ag-NPs were attached via Ag-S [43]. The addition of cysteine with the Ag^+ behaved as a suitable example of controlling the levels of silver [32], because cysteine acted as a bridging agent for the binding of Ag-NPs.

2.3.4 Incorporation of Silver Nanoparticles onto Cellulose Acetate Membranes

Glycidyl methacrylate (GMA) is a low-cost epoxy widely used in industrial products, such as coatings and adhesives [97] because its vinyl groups can be graft onto functional surfaces [8, 98]. Epoxides are known to have highly reactive functional

groups due to the strained three-membered ring of GMA, and are susceptible to a large range of nucleophiles [99]. With GMA's epoxy end, a large number of covalent attachments can be formed with ligands, such as amines, carboxylic acids, hydroxyls, pyridines, and peptides [100]. Wang et al. showed that poly-GMA can be attached to CA via the hydroxyl groups [101], allowing additional possible functionalization to occur. The majority of primary and secondary amines were able to attach to the epoxide ring without the use of catalysts. However, solvent choice was a crucial factor to the S_N2 ring-opening reaction (*Fig. 2.8*) because the solvent polarity directly affected the conversion of the epoxide and vinyl terminal groups. DMSO has been found to act as a good solvent for many hydrophobic and hydrophilic primary amine reagents [99]. By using DMSO, a steady transition state of the S_N2 reaction progressed between the epoxy group of the GMA and amine group of the cysteamine (C_2H_7NS) [8]. DMSO is an aprotic, polar solvent, where the solvent cannot donate hydrogens. Studies have shown that cysteamine is suitable for crosslinking reactions with GMA; however, cysteamine amine and thiol groups can unintentionally graft onto the epoxide groups of the poly-GMA [102]. Research shows that there are strong silver and thiol interactions through covalent bonding [8, 28, 31, 37, 102]. Therefore, by imitating silver attraction towards the thiol groups of cysteines found in bacteria, it is hypothesized that the same mechanism can be applied in modifying CA/GMA membranes to bind Ag-NPs to the membranes.

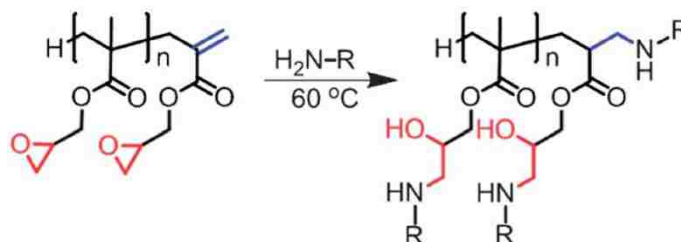


Figure 2.8: Attachment of poly-GMA with primary amine via S_N2 reaction [99]

3 OBJECTIVES

The scope of this research was to functionalize CA membranes with Ag-NPs to produce low-biofouling ultrafiltration (UF) membranes for potential pretreatment for other filtration process, such as reverse osmosis RO, by retaining colloids, microorganisms and macromolecules [48]. Desalination by RO is costly and requires pre-treatment, so the use of UF can make the process much more economically attractive [48].

To this end, this study included functionalizing cellulose acetate (CA) membranes with both physically (^PAg-NP) and chemically (^CAg-NP) attached silver nanoparticles (Ag-NPs) to make them less prone to biofouling. The membranes were characterized accordingly for their modification and properties through a variety of instrumentation. In addition, the biofouling effects of bacteria were observed through controlled studies to induce biofilm growth in order to understand the mechanism more. To achieve this, the following tasks were performed.

3.1 Characterization of the Ag-NPs.

- a) Ag-NPs were analyzed for particle sizing and distribution with transmission electron microscope (TEM).

3.2 Physical Attachment of the Ag-NPs.

- a) Cellulose acetate (CA) polymer and silver nanoparticles (Ag-NPs) were blended in dope solution via sonication.

3.3 Chemical Attachment of Ag-NPs (^CAg-NP/CA) onto the Membranes.

- a) Glycidyl methacrylate (GMA) was polymerized by using benzoyl peroxide (BPO) and toluene to facilitate free radical initiation.
- b) CA and polymerized GMA (poly-GMA) were blended together with NMP solvent via dope solution to graft homopolymerize the poly-GMA onto the hydroxyl groups of CA.
- c) Surfaces of the copolymer CA/GMA membranes were bounded with cysteamine (CYS) to the epoxy ring of GMA via S_N2 reaction through bath immersion.
- d) Ag-NPs were crosslinked to the surface of the functionalized CA/GMA/CYS membrane via bath immersion.

3.4 Characteristics of the CA, ^PAg-NP/CA, and ^CAg-NP/CA Membranes.

- a) X-ray photoelectron spectroscopy (XPS) was used to detect membrane modifications, the presence of silver and determine which chemical elements are present on the membrane surfaces.
- b) CA, ^PAg-NP/CA, and ^CAg-NP/CA membranes were subjected to dead-end filtration experiments for flux, bacterial cell adhesion and salt rejection.
- c) Drop test analyzer was used on CA, CA/GMA, CA/GMA/CYS, ^PAg-NP/CA, and ^CAg-NP/CA membranes to analyze the contact angle and hydrophilicity (Kruss).
- d) The durability of Ag-NP attachment was determined using inductively coupled plasma optical emission spectroscopy (ICP-OES) to study silver leaching studies from cross-flow filtration with ^PAg-NP/CA and ^CAg-NP/CA membranes.
- e) Scanning electron microscope (SEM) coupled with X-ray energy dispersive spectroscopy (EDX) were used to detect the presence of silver and for the membrane's structural morphology.

3.5 Effects of Biofouling on CA, ^PAg-NP/CA, and ^CAg-NP/CA Membranes.

- a) CA, ^PAg-NP/CA, and ^CAg-NP/CA membranes were subjected to controlled filtration experiments to induce increased biofilm formation.
- b) Biofouled membranes were stained with NucBlue and propidium iodide (PI) for live/dead cell counts of detached cells and observed with fluorescence microscopy.

4 MATERIALS AND METHODS

4.1 Materials

4.1.1 Glassware

All glassware used (graduated cylinders, volumetric flasks, Erlenmeyer flasks, vials, PYREX® media storage container, etc.) were subjected to a detergent wash followed by three rinses with distilled water and acetone. The distilled (DI) water was provided by a Purelab Flex 3 filtration system (Elga, Illinois, USA). For bacterial experiments, all necessary glassware was autoclaved for 30 minutes to ensure sterilization and covered with aluminum foil or Parafilm until use.

4.1.2 Chemical Reagents

Membranes were cast using cellulose acetate (CA, average Mn ~30,000) purchased from Sigma Aldrich (St. Louis, MO), glycidyl methacrylate (liquid, GMA, 97% stabilized with 100 ppm 4-methoxyphenol) purchased from Alfa Aesar (Haverhill, MA) and N-methyl-2-pyrrolidinone (NMP, for peptide synthesis) purchased from Millipore (Massachusetts, USA). The monomer GMA was polymerized with toluene (HPLC UV-grade) purchased from Pharms-AAPER (Shelbyville, KY) and benzoyl peroxide (97% dry wt., wet with 2.5% water) purchased from VWR (Pennsylvania, USA). Functionalizing the epoxide groups of the poly-GMA was accomplished by the use of 2-aminoethanethiol (or cysteamine) purchased from TCI (Oregon, USA) and dimethyl sulfoxide (DMSO) purchased from VWR.

4.1.3 Silver Nanoparticles (Ag-NPs)

The Ag-NPs (70.37% w/w Ag⁰) incorporated into the membranes were casein-coated and provided by Professor Vinka Craver from the University of Rhode Island through Argenol labs (Zaragoza, Spain).

4.1.4 Bacterial Analyses Materials

Nutrient agar and agar plates were made from nutrient broth solution purchased from VWR and M877-500 G standard nutrient agar purchased from HIMEDA (Mumbai,

India). The synthetic brackish water was made from InstantOcean sea salt purchased from PetSmart (Kentucky, USA). Bacterial strain, #13525 *Pseudomonas fluorescens* Migula, was purchased from ATCC (Virginia, USA). *Pseudomonas fluorescens* biofilms has been studied with FTIR and peak locations of different components are known [103]. Sodium acetate and 2-propanol were purchased from Sigma-Aldrich. Acetone was purchased from VWR, ethanol was purchased from Millipore and propidium iodide (PI) was purchased from Invitrogen (California, USA). Concentrated hydrochloric acid UN1789 and NucBlue® live cell stain readyprobes™ reagents were purchased from Fisher Scientific (Pennsylvania, USA). The PI and NucBlue® live cell stain readyprobes™ reagents were used as received. Permeates from the leaching studies were collected in Corning® sterile centrifuge tubes, provided by Environmental Research Training Laboratories (ERTL) from University of Kentucky (Kentucky, USA).

4.2 Methods

4.2.1 Polymerization of GMA

The polymerization of the monomer GMA (mono-GMA) (Fig. 4.1) was achieved with a two-necked round bottom flask, Fig. 4.2a. For each reaction, 15 mL mono-GMA, 35 mL toluene, and 0.10 g benzoyl peroxide were combined into the round bottom flask with a stir bar and kept under a nitrogen atmosphere to prevent undesired oxidation and side reactions from occurring, Fig. 4.2b [15, 98]. The reaction was kept under constant temperature of 65-70°C (J-Kem Scientific Model 250 Digital Temperature Controller, St. Louis, MO) for 2-6 hours with continuous stirring.

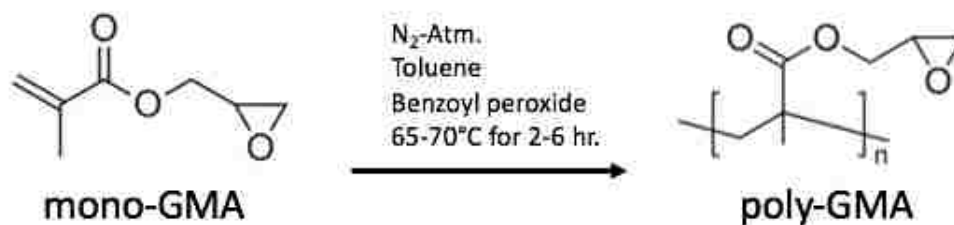


Figure 4.1: Glycidyl methacrylate polymerization reaction scheme

The product was collected from the flask, dried, and crushed over a period of a week, *Fig. 4.3*, and a desiccator was used to speed up the drying process. The use of a FTIR confirmed the polymerization reaction via the disappearance of the carbonyl bond ($C=O$, $\sim 1720\text{ cm}^{-1}$) and the appearance of epoxide groups (758 cm^{-1} , 843 cm^{-1} , 905 cm^{-1} , and 1254 cm^{-1}) [104].

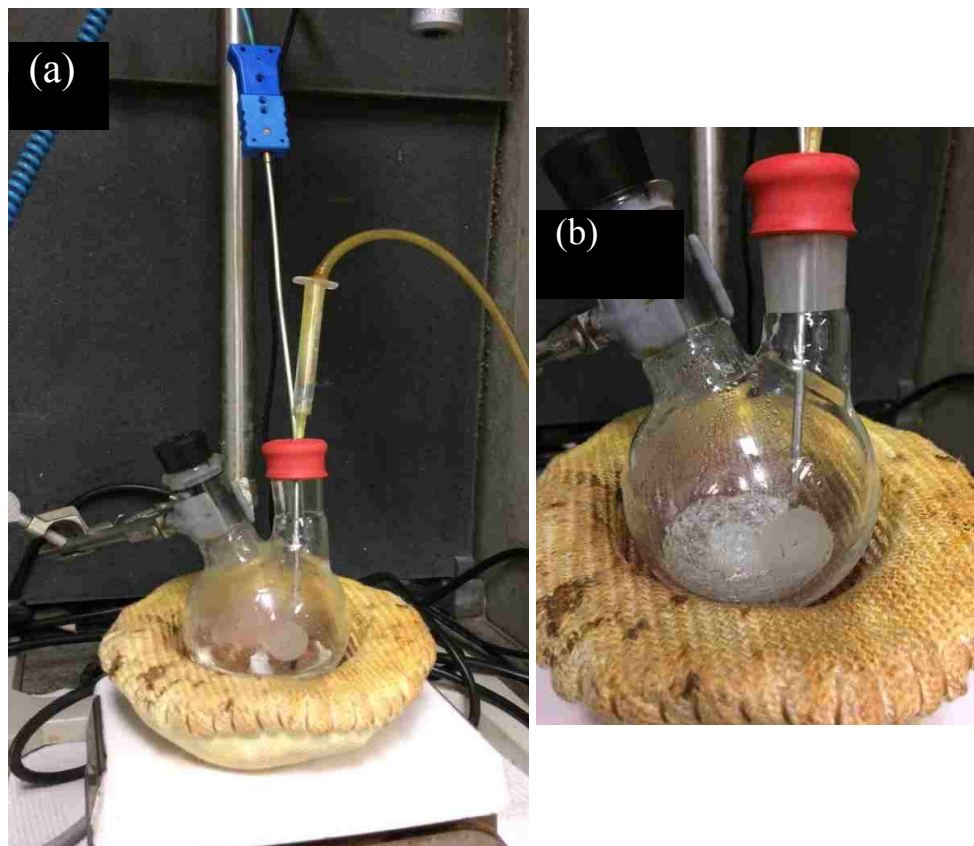


Figure 4.2: Experimental setup of mono-GMA polymerization reaction



Figure 4.3: Drying crushed polymerized GMA product over a week

c

4.2.2 Membrane Casting

All membranes were made in a dope solution, consisting of a polymer, solvent (NMP) and additives (such as GMA or nanoparticles). Asymmetric membranes were made using phase inversion via immersion precipitation in a water bath. *Fig. 4.4* shows the process of casting a membrane where first, the dope solution was poured across a glass substrate (*Fig. 4.4a-b*), and cast using a doctor blade (Paul N. Gardner Pompano Beach, FL US PAT 4869200) to obtain an approximate thickness of 120-130 μm (*Fig. 4.4c*) [21]. This was then immersed in a water bath to allow the exchange of solvent (NMP) and non-solvent (water) (*Fig. 4.4d*), which took up to 10-15 minutes [21].

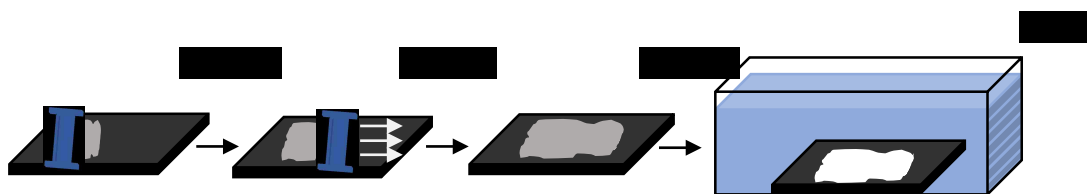


Figure 4.4: Fabrication of a membrane through phase-inversion process

4.2.3 Fabrication of Cellulose Acetate (CA) Membranes

CA dope solutions consisted of 18/82 CA/NMP wt.% [15, 21]. Both the polymer and solvent were sonicated together overnight, or until the solution became clear. Then, the solutions were degassed for 60 minutes prior to casting to remove any present air bubbles. Membranes were then cast as previously described.

4.2.4 Fabrication of Physically Attached Ag-NPs (^PAg-NP)/CA Membranes

^PAg-NP/CA dope solutions consisted of 18/0.25/82 CA/Ag-NPs/NMP wt.% [15]. The Ag-NPs and NMP solvent were sonicated together for about 30 minutes until a dispersed black solution was obtained, and then the CA powder was added to the dope. The dope solution was sonicated overnight and degassed for 60 minutes before being cast into a membrane. Prior to each additional casting of the membranes, the dope solutions were sonicated/degassed for 10 minutes to ensure dispersion of the Ag-NPs to create more uniform membranes, and membranes were cast as previously described.

4.2.5 Fabrication of CA/GMA Membranes

CA/GMA dope solutions consisted of 18/80/2 CA/NMP/GMA wt.% ratio [15]. Both the CA and GMA polymer (crushed into small pellets) were blended together with the NMP solvent overnight, or until the solution became clear, and cast as previously stated. The reaction scheme can be followed below, *Fig. 4.5*. Again, membranes were then cast as previously described.

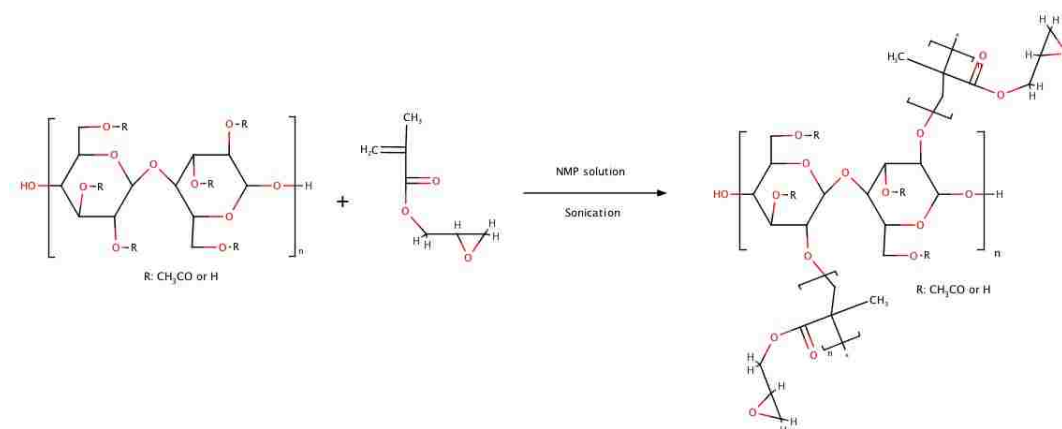


Figure 4.5: Fabrication of CA/GMA membranes

4.2.6 Fabrication of Chemically Attached Ag-NPs (^CAg-NP)/CA Membranes

^CAg-NP/CA membranes were made through a series of reactions, *Fig. 4.6*. First, flat sheet CA/GMA membranes were immersed in solution baths of 0.1M cysteamine (CYS) and 50/50 water/DMSO for 2-6 hours, *Fig. 4.6a*. The bath temperature was set for 50-55°C to facilitate the attachment of the primary amine on the end of the GMA's epoxide groups [99]. Then, the membranes were rinsed with copious amount of DI water and placed in a 0.25% Ag-NPs bath (by wt.%) for 24 hours (*Fig. 4.6b*). After 24 hours, the ^CAg-NP/CA membranes were rinsed with copious amount of DI water and stored in DI water. Based on other studies, there are strong silver and thiol interactions through covalent bonding [8, 28, 31, 37, 102], and it was expected that there would be Ag-S bonding in these reactions.

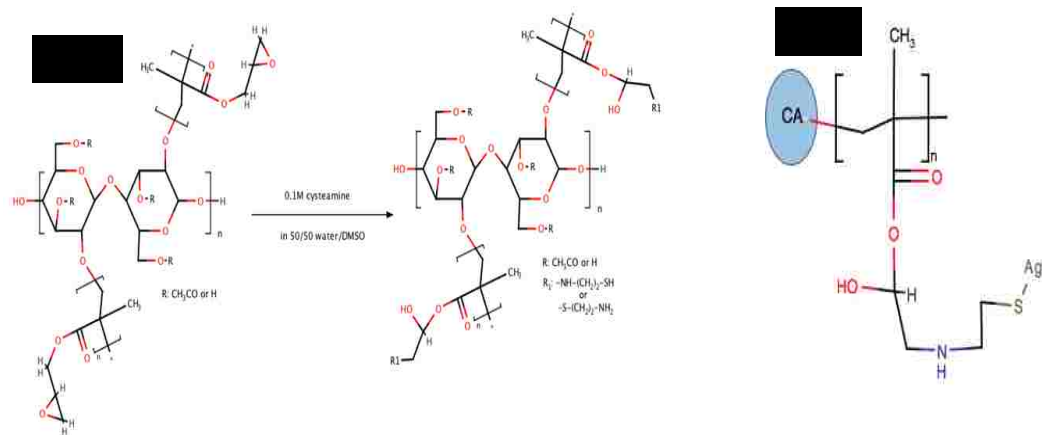


Figure 4.6: Fabrication of chemically attached Ag-NP/CA membranes

4.3 Chemical and Morphological Characterization

4.3.1 Transmission Electron Microscope

Silver nanoparticle size distribution was analyzed using transmission electron microscope (TEM) (JEOL 2010F, Tokyo, Japan). In order to analyze the nanoparticles (NPs), a 1/10000 Ag-NPs solution by mass in distilled water was used. The sample was prepared on TEM copper grids (Lacey Carbon Type-A, 300 Mesh, Copper Catalog #01895 Vendor: Ted Pella). A single drop of the diluted Ag-NPs solution was applied onto the grid and any excess water was siphoned off with a Kimwipe tissue. The copper grid sample was dried for 4 days to get rid of any moisture that might have been left on the grids.

4.3.2 Fourier Transform Infrared (FTIR) Spectroscopy Analysis

FTIR analysis was performed in attenuated total reflectance (ATR) mode Thermo Scientific Fourier transform infrared spectroscopy (Massachusetts, USA). The contact crystal (diamond) was cleaned well with isopropanol before each sample use. Each membrane was analyzed in three areas. FTIR provides information regarding the chemical structure and progress of reactions for a sample. FTIR analysis was used to provide verification of the GMA polymerization reaction.

4.3.3 X-ray Photoelectron Spectroscopy

Membrane surfaces were analyzed using a K-Alpha X-ray photoelectron spectroscopy (XPS) (Thermo Scientific, Massachusetts, USA) for elemental compositions based off corresponding binding energies excited by the x-ray beam. All samples were freeze-dried before use to remove any moisture. The S_{2p}, C_{1s}, Ag3d_{5/2}, Ag3d_{3/2}, N_{1s}, and O_{1s} core level peaks were the main focus. It should be noted that exact chemical structures binding energies are exclusive and possible misinterpretations of the chemical structure are possible due to local variations in the data [105].

4.3.4 Scanning Electron Microscope/Energy-dispersive X-ray Spectroscopy

Analysis of the surfaces and cross-sections of the membranes was performed using various scanning electron microscopes (SEM) (Zeiss EVO, Oberkochen, Germany, Quanta FE / Environmental SEM, Oregon, USA, and Hitachi S4300 FE-SEM, Berkshire, United Kingdom) and with energy-dispersive x-ray spectroscopy (EDX). SEM/EDX was used to image membrane surfaces and biofouling. Cross-section membrane samples were prepared by freezing the membrane overnight, followed by liquid nitrogen immersion for 5 minutes to make them brittle. The samples were carefully snapped in half, to help ensure the morphology of the inside was unaffected. Surface-section membranes were prepared by freezing the sample overnight, then placing in a Freeze Dryer (Labconco, Missouri, USA) to remove all moisture. All samples were sputtered with palladium-gold (Quorum Emscope SC400, Laughton, United Kingdom) for 5 minutes prior to electron imaging to help prevent charging of the membranes. The EDX mode was used to analyze and quantify compositional elements that might be on the membrane.

4.3.5 Contact Angle

All membranes were analyzed using a Drop Shape Analyzer (Krüss, Hamburg Germany) to measure hydrophilicity. An observed increase in contact angle corresponds to a decrease in hydrophilicity [30]. Prior to testing, each membrane sample was patted dry with a Kimwipe tissue. Each sample had 10-15 readings to account for accuracy of the measurements. A program was set within the instrument itself to take readings for 10

seconds with 2 frames per second (fps) as soon as the water droplet made contact with the membrane surface. All measurements were averaged accordingly.

4.4 Permeability, Selectivity and Fouling Studies

4.4.1 Bacteria Growth and Harvesting

The bacteria used for filtration were harvested after 48 hours to obtain an approximate 10^9 cells/mL count. These cells were grown overnight in 20 mL sterile nutrient agar in an incubator set for 30°C. To achieve the count of 10^4 cells/mL necessary for the permeation studies, the cell solutions were serially diluted as necessary. Plate counting of the cells was performed regularly to ensure the counts remained close to the 10^4 cells/mL counts. According to previous studies [15], this count, when harvested at the late exponential growth phase, is able to effectively create an EPS biofilm layer.

4.4.2 Permeability Studies

Flux decline studies were performed using a 10 mL Amicon dead-end filtration cell 8010 (EMD Millipore, Massachusetts, USA), *Fig. 4.7*. Dead-end filtration was used to enhance biofouling by concentrating bacteria close to the membrane surface; thus, experiments could be performed with lower feed solution volume and shorter periods of time as compared to cross-flow filtration. The cell has an area of 4.1 cm², and the membranes were cut and placed into this slot for the experimental runs. To prevent accidental cracking or tearing of the membranes, the membranes were placed on top of a support layer, or filter paper. All readings were performed at constant volume measurements of 2 mL at a constant pressure of 4.14 bars (60 psi) to imitate ultrafiltration pressure processes and kept with constant stirring to keep the solution dispersed.

Each experiment began with constant volume precompaction using 20 mL of DI water for 2-6 hours. Precompaction was performed as a means for the membrane to reach steady flux before filtration [106]. Precompaction was followed by filtration of synthetic brackish water with 10^4 cells/mL *Pseudomonas fluorescens* Migula for 4-10 hours (20 mL). Lastly, reverse flow filtration was performed for 1 hour at 2.07 bars (30 psi) to remove any foulants not adsorbed to the membrane surface (i.e. remove reversible

foulants). Flux was recorded as L/m²hr and plotted versus time since experiments were operated under constant pressure. Flux recovery for the experiments was determined by: where J_f and J_i represents the final and initial flux, respectively.

$$\text{Flux Recovery (\%)} = \frac{J_f}{J_i} * 100\%$$

All experiments were performed at least three times for reproducibility.

InstantOcean salt was used to reproduce synthetic brackish water since it is comparable to natural seawater [107]. A concentration of 10% was used, which was approximately 1 part InstantOcean salt and 317 parts DI water (3 mL InstantOcean salt/1L DI water).

Table 4.1 provides the concentration of major cations and anions found InstantOcean salt and seawater.

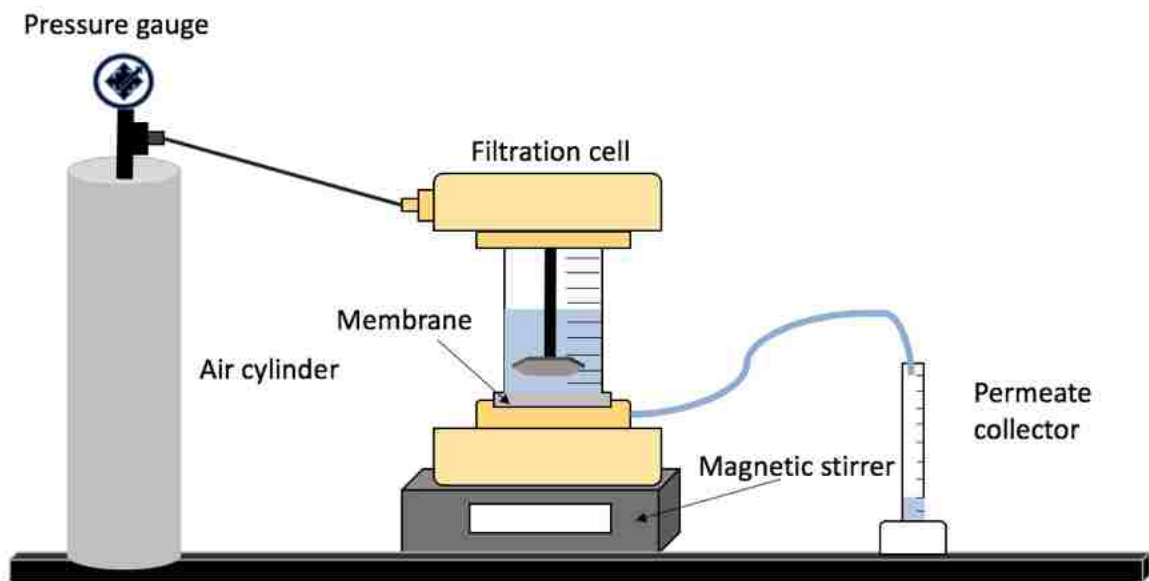


Figure 4.7: Dead-end filtration schematic

Table 4.1: Major cations/anions compositions of synthetic brackish and seawater for comparison [107-109]

Component	Composition of InstantOcean salt (ppm)	Composition of Seawater salt (ppm)
Na ⁺	10,621	10,805
K ⁺	368	399
Mg ²⁺	1,264	1,288
Ca ²⁺	377	413
Sr ⁺	17	8
Cl ⁻	18,469	19,498
SO ₄ ²⁻	2209	2690
TCO ₂	247	247

4.4.3 Salt Rejection

Each salt rejection experiment began with constant volume precompaction of DI water for 1 hour. Filtration of synthetic brackish water (3 mL InstantOcean salt/1L DI water) followed until 4 mL was obtained. All readings for salt rejections were performed at constant pressure of 4.14 bars (60 psi). A 09-330 conductivity probe (Fisher Scientific, Pennsylvania, USA) was used to determine electrical conductivity present in water caused by salts and other ions. The permeate and feed solution from the filtration studies were collected and analyzed with the conductivity probe for differences in ion concentrations. Salt rejection was calculated using:

$$\text{Salt Rejection (\%)} = \left(1 - \frac{C_p}{C_f}\right) * 100\%$$

where C_p represents the solute concentration in the permeate and C_f represents the solute concentration in the feed solution.

4.4.4 Silver Leaching Crossflow Studies

^CAg-NP/CA, and ^PAg-NP/CA membranes were placed inside a modified flow cell (actual cell size: 80 mm x 100mm, *Fig. 4.8a*) and 500 mL of DI water was passed through using a peristaltic pump (Manostat Vera, USA) at a flowrate of 70.38 mL/min, *Fig. 4.8b-c*. This study was performed to monitor any form of silver leaching that might have detached from the membranes, according to procedures previously used [8]. The water was passed over the membranes (dimension of membrane required: 40 mm x 76

mm) inside the flow cell, into a recycling reservoir and passed through repeatedly, *Fig. 4.8c*. The reservoir was stirred constantly with a magnetic stirrer to ensure dispersion of any ions that might have been present in the water. The membranes were placed between two plastic grid spacers inside the flow cell to help create turbulence for the water flow. 5 mL sample aliquots were collected at various time intervals for a week during the crossflow studies. In order to prevent any possible bacterial degradation of silver, two drops of concentrated HCl were added to sample aliquots, which were stored in a dark fridge.

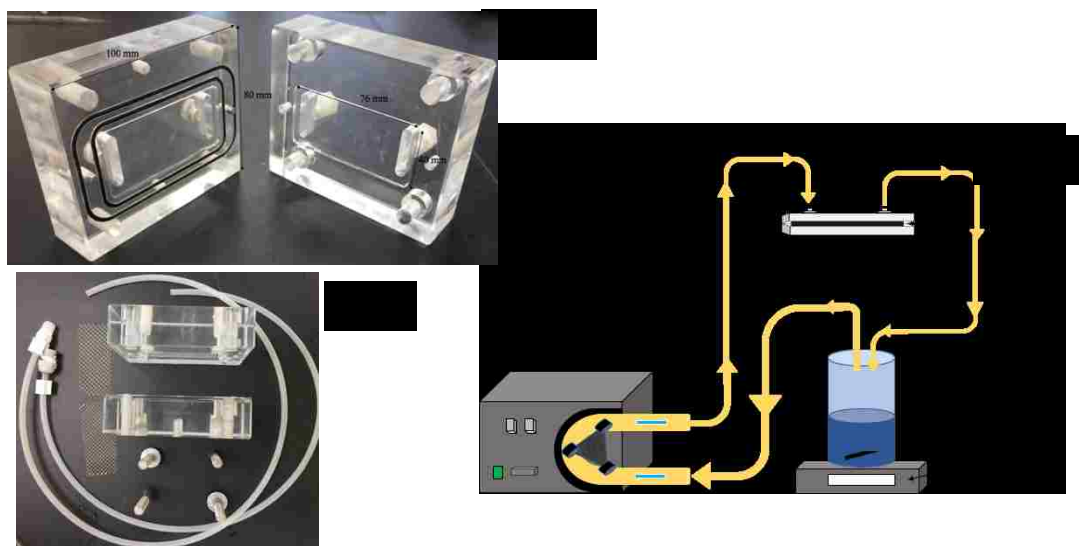


Figure 4.8: Crossflow filtration parts and schematics

A Vista-Pro Ion Coupled Plasma Optical Emission Spectroscopy (ICP-OES) (Varian Inc., Palo Alto, USA), equipped with argon plasma and a CCD detector, was used to determine the concentration of silver that leached from the membranes. The instrument is capable of measuring concentrations down to the parts per billion (ppb). A 1000 $\mu\text{g}/\text{mL}$ Ag standard (Environmental Express, Ag Silver 1000 $\mu\text{g}/\text{mL}$ CAT#HP100051-1) was serially diluted with 2% nitric acid into 0.02, 0.05, 0.10, 0.5, 1 and 5ppm solutions to create a calibration curve, which was used to accurately determine the concentration of silver present in the solutions. To ensure matrix matching of the samples and standards, all solutions were ensured to be 5% nitric acid total composition.

4.4.5 48-Hour Biofouling Studies

CA, ^PAg-NP/CA, and ^CAg-NP/CA membranes were subjected to 48-hour controlled filtration experiments using a 350-mL dead-end filtration Amicon cell with maximized biofilm formation conditions. Feed solutions consisted of 350 mL synthetic brackish water with 10⁴ microbial cells/mL and 30 mg/L of sodium acetate as nutrient source. A pressure of 0.69-1.03 bars (10-15 psi) was used, and no flux values were recorded.

All filter cells and beakers used for these biofouling experiments were sprayed with high proof ethanol to reduce possible contamination. The studies were performed to evaluate the efficiency of Ag-NPs in controlling membrane biofouling when either physically dispersed or chemically attached to membranes. All experiments were performed at least three times for reproducibility.

After 48 hours of filtration, the membranes were rolled up and placed in Corning® sterile centrifuge tubes containing 12 mL of synthetic brackish water, and were sonicated for 40 minutes to detach cells. Then, 1 mL aliquots were taken from the test tube, placed in sterile Corning® centrifuge tubes and stained accordingly (two drops of NucBlue® live cell stain readyprobes™ reagents stain and one drop of propidium iodide per mL of sample). Once samples were stained, they were left at room temperature for 30 minutes (incubation time required for stains) and then analyzed using fluorescent microscopy. Several areas of the media solution were observed. Contamination was minimized by spraying surfaces with high proof ethanol.

4.4.6 Fluorescence Microscopy

An Eclipse Ti fluorescence microscope (Nikon, New York, USA) was used to observe live/dead cells from the 48-hour biofouling studies. There were three available filters on the microscope: UV for blue, B for green, and G for red fluorescence dyes/stains. These filters were for specific excitation and emission wavelengths based on the characteristics of the stains used for the cells. 40µL aliquots of stained samples from the 48-hour fouling studies were placed on a glass microscope slide and viewed under the microscope. The NucBlue stains (to observe live cells) were examined under the UV filter mode, while the propidium iodide (PI) (to observe dead cells) were examined under

the G filter mode. Several areas of the sample media were examined and recorded under corresponding filter modes with an analog gain of 1x, to control the emission signal and necessary exposure noise.

5 RESULTS AND DISCUSSION

5.1 Characterization of the Silver Nanoparticles

5.1.1 Determining Particle Size and Distribution

Nanoparticle properties are dependent on size, extent of dispersion, and structure [36]; therefore, the relative size of the nanoparticles were determined. To this end, TEM images of dried casein-coated Ag-NPs (*Fig. 5.1a*) and particle size distribution (*Fig. 5.1b*) were obtained. Casein-coated Ag-NPs were found to be predominantly spherical in nature with a particle size distribution of 12.3 ± 1.9 nm, which agreed with previous studies by Kallman et al. and Zhang et al. that found their sizes to be 15 nm and 12.6 ± 5.7 nm respectively [4, 33]. Ag-NPs with sizes of 10-100 nm have been found to exhibit good disinfection properties [110] since smaller nanoparticles can penetrate cells more easily to disrupt their respiration [7, 13, 33, 35, 36, 84-86].

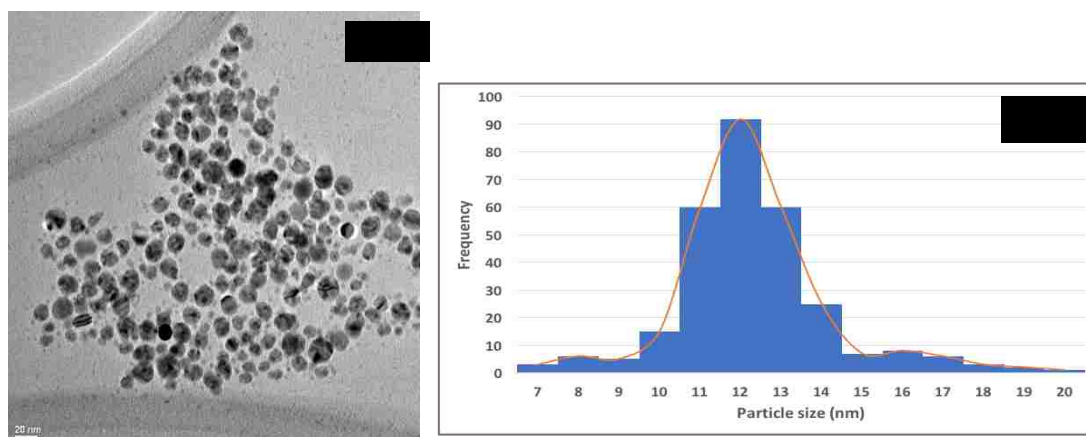


Figure 5.1: (a) TEM images of dried casein-coated Ag-NPs and (b) particle size distribution

5.2 Membrane Functionalization with Silver Nanoparticles

The overarching goal of this study was to functionalize CA membranes with Ag-NPs to produce low-biofouling membranes for potential pretreatment processes. Immobilizing Ag-NPs on membranes reduces the amount of leaching; however, it also decreases the available interaction sites to potentially decrease their antimicrobial function. Therefore, an immobilization technique was sought that would simultaneously prevent silver nanoparticle leaching while maintaining its antimicrobial function. The

functionalization of Ag-NPs onto the CA was achieved via attachment with functionalized thiol groups. Thiol groups were chosen as an attempt to imitate the biocidal nature of Ag^+ where the metal attaches to thiol groups that make up many bacterial structures [20, 22, 31].

Eighteen percent CA membranes were cast as baseline for performance and comparison with silver nanoparticle membranes. The first set of membranes developed here were 18% CA membranes with 0.25 wt.% Ag-NPs physically-blended in the dope solution ($^{\text{P}}$ Ag-NP/CA membranes). The second set were the membranes with Ag-NPs chemically attached to CA membranes ($^{\text{C}}$ Ag-NP/CA membranes). These membranes were made by homopolymerizing CA polymer and poly-GMA in coarse powder form in the solvent solution through sonication to create the CA/GMA membranes. The CA/GMA membranes were incorporated with thiol groups via cysteamine addition reaction, as shown in *Fig. 5.2*, followed by the attachment of thiol groups from cysteamine to form CA/GMA/CYS membranes (*Fig. 5.3a*) and lastly covalently attached to Ag-NPs to create $^{\text{C}}$ Ag-NP/CA membranes (*Fig. 5.3b*).

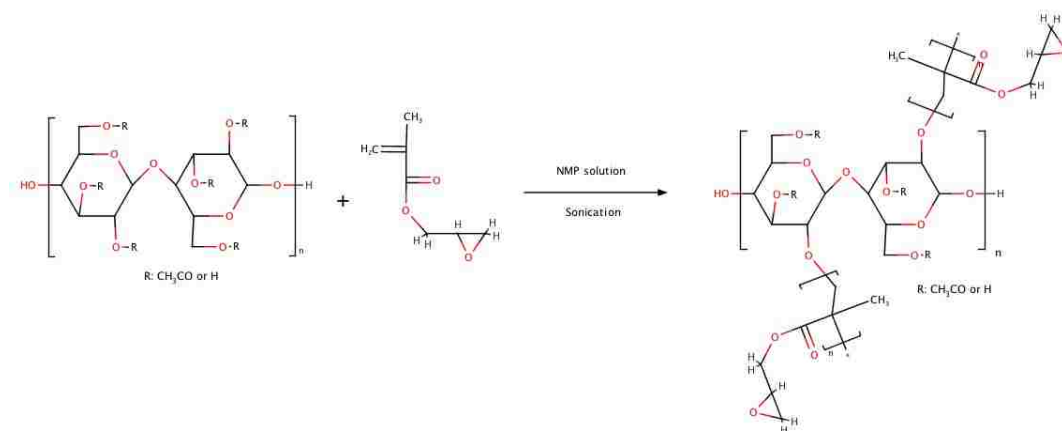


Figure 5.2. Proposed reaction of CA with GMA to form CA/GMA membranes

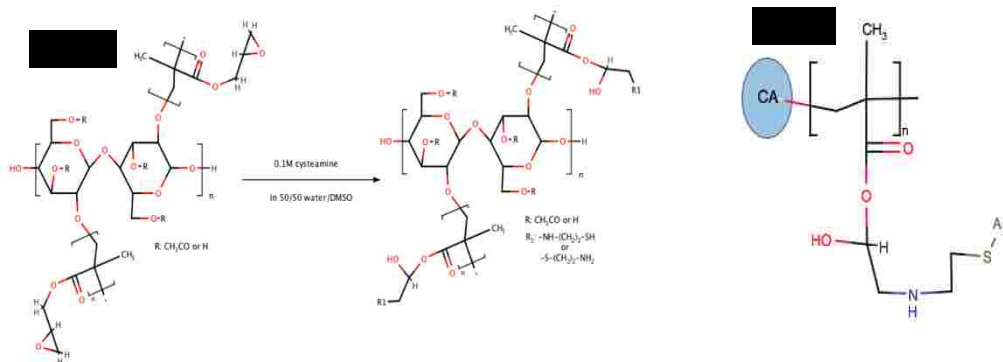


Figure 5.3 Fabrication of ^CAg-NP/CA membranes

5.3 Characterization and Morphology of the CA and Modified Membranes

5.3.1 Polymerization of GMA

The monomer GMA (mono-GMA) was polymerized (poly-GMA) using toluene and benzoyl peroxide, and reacted under nitrogen atmosphere, to avoid undesired side reactions [15, 98]. Mono-GMA underwent phase transformation from a liquid to a hard epoxy due to the polymerization reaction. To verify polymerization of mono-GMA to poly-GMA, ATR-FTIR was performed. As shown in *Fig. 5.4* and *Table 5.1*, stretching of C=O (1720 cm^{-1} [111]), epoxy (906 cm^{-1} [111]), C=C (1636 cm^{-1} [104]), and two CH₃ bands (1448 cm^{-1} , and 1484 cm^{-1}) were observed. Epoxy groups were present at 758 cm^{-1} , 843 cm^{-1} , 905 cm^{-1} , and 1254 cm^{-1} [104]. The FTIR absorption bands of the aforementioned peaks (758 cm^{-1} , 843 cm^{-1} , 905 cm^{-1} , and 1254 cm^{-1}) showed reasonable retention of the epoxide groups between the monomer and polymer. The disappearance of the C=C stretching band, 1636 cm^{-1} , from the poly-GMA spectrum verified completion of the polymerization reaction [104] since mono-GMA possesses this characteristic C=C bond next to its ester group. This suggests the polymerization reaction path favored the vinyl groups of the monomer and created the sequencing chain lengths for the polymer [104].

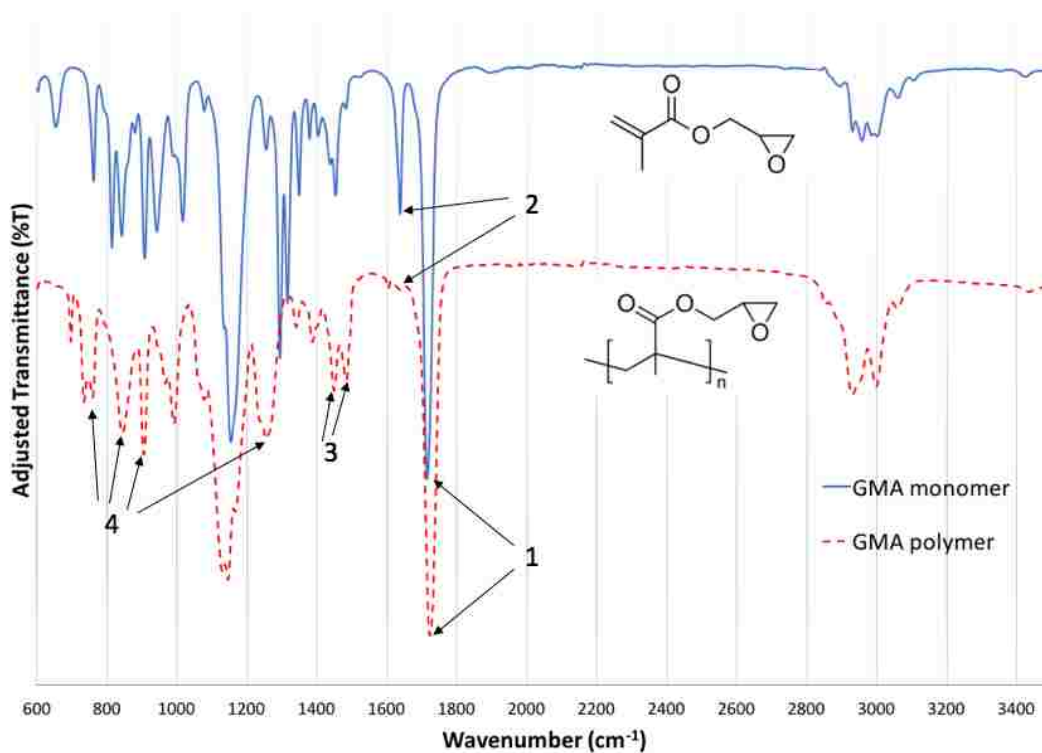


Figure 5.4: Progression of the GMA polymerization reaction

Table 5.1: Corresponding functional groups and wavenumber for FTIR spectra

<i>Band Number</i>	<i>Functional group</i>	<i>Wavenumber (cm⁻¹)</i>
1	C=O	1720
2	C=C	1636
3	CH ₃	1448, 1484
4	epoxy ring	758, 843, 905, 1254

5.3.2 Verification of Membrane Functionalization

Completion of membrane functionalization steps for ^CAg-NP/CA membranes was verified using XPS, as shown in Fig. 5.5. The atomic percentages (At.%) were calculated from the XPS peaks and are shown in Table 5.2. The progress of reactions was based off the reaction schemes shown in Fig. 5.2 and Fig. 5.3a,b.

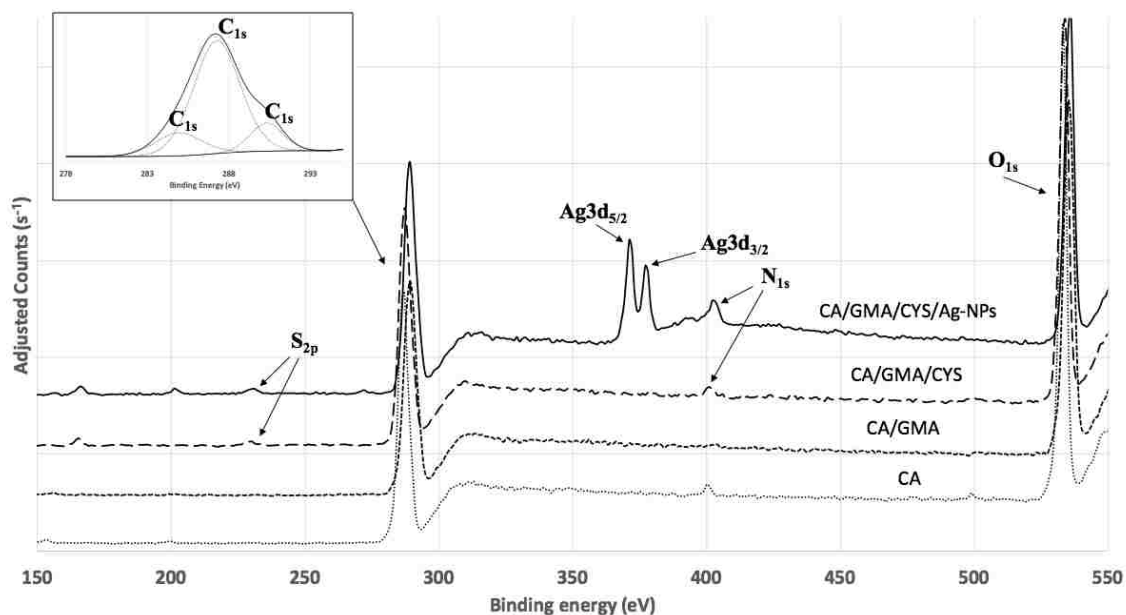


Figure 5.5: XPS spectra (150-550 eV) of CA, CA/GMA, CA/GMA/CYS and CA/GMA/CYS/Ag-NPs membranes with corresponding core level peaks

XPS spectra showed the presence of nitrogen in membranes that did not contain it, such as CA and CA/GMA membranes. The presence of nitrogen might have been due to surface contaminations [112] or to biological attack of stored samples [105]. Therefore, nitrogen peaks were not used to verify reaction completion. *Fig. 5.5* and At.% shown in *Table 5.2* demonstrated that the addition of cysteamine (CYS) produced a sulfur S_{2p} and N_{1s} peak, which was expected since CYS molecular formula consist of C_2H_7NS . From the addition of Ag-NPs, two silver peaks were observed ($Ag3d_{5/2}$ and $Ag3d_{3/2}$), plus S_{2p} and N_{1s} in the top spectrum, while none for previous steps of the reactions. The proposed silver attachment reaction was confirmed and analyzed by XPS by performing three separate cAg -NP/CA membranes in three separate reactions to ensure reproducibility. The combined At.% for the elements S and Ag from these reactions were analyzed and obtained as followed: $0.75 \pm 0.23\%$ and $0.83 \pm 0.63\%$ respectively.

Table 5.2: Atomic % of the reaction scheme to create ^CAg-NP/CA membranes

Total elemental composition	Atomic %			
	CA	CA/GMA	CA/GMA/CYS	CA/GMA/CYS/Ag-NPs
Carbon	61.67	59.76	62.79	62.59
Oxygen	37.05	39.51	35.14	33.09
Nitrogen	1.27	0.73	1.32	3.21
Sulfur	-	-	0.76	0.60
Silver	-	-	-	0.51

5.3.3 Membrane Morphology and Structure

Membrane cross sections were observed using SEM imaging, as shown in *Fig. 5.6*. More channels were visible in the ^PAg-NP/CA membrane (*Fig. 5.6b*), as compared to CA (*Fig. 5.6a*) and ^CAg-NP/CA (*Fig. 5.6c*) membranes. It has been speculated that NPs might act as pore forming agents during the phase inversion process [90] due to the hindrance effect of the NPs [90, 91]. When added to the dope solution, nanoparticles have also been shown to agglomerate during the phase inversion process, which might have contributed to macrovoid growth of the membranes [113]. Therefore, the appearance of more open channels on ^PAg-NP/CA membrane could be due to the Ag-NPs, and this was hypothesized to correspond to higher permeability of the membranes, as was observed in the permeability studies discussed later. ^CAg-NP/CA membranes did not seem to share these morphology characteristics, which may have been due to the fact the Ag-NPs were attached via post-functionalization in a bath.

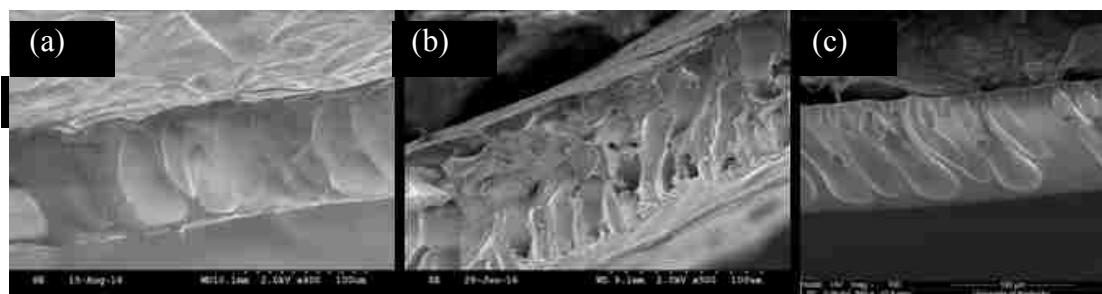


Figure 5.6: Cross section SEM images of (a) 18%CA, (b) ^PAg-NP/CA and (c) ^CAg-NP/CA membranes

The surface morphology of membrane pores was also imaged through SEM. CA and ^PAg-NP/CA membranes appeared to have similar morphology with sponge-like honeycombed pores (*Fig. 5.7a-b*), which was hypothesized to provide more flow pathways [21]. On the other hand, the ^CAg-NP/CA membranes appeared to have tighter pores with thicker networks, which may have been due to GMA's ability to bind with many types of nucleophiles, and ultimately create more crosslinking between the polymers [99]. Blending polymers has the potential to create different pore structures and new binding sites [15]. It was expected that higher occurrences of crosslinking would give lower water permeation [114], which may explain the lower permeation of the ^CAg-NP/CA membranes, compared to the other two membranes, as discussed later in *Section 5.4.1*. When comparing the surface and cross-section SEM images of the CA membranes (*Fig. 5.6a* and *Fig. 5.7b*) with the ^PAg-NP/CA and ^CAg-NP/CA membranes, the presence of more open channels on the ^PAg-NP/CA cross-section (*Fig. 5.6b*) suggests higher permeation, likely due to the nanoparticles acting as pore formers. On the other hand, the tighter pores of the ^CAg-NP/CA membranes (*Fig. 5.7c*), likely due to additional crosslinking, suggests lower permeability but higher selectivity as compared to the other membranes [115].

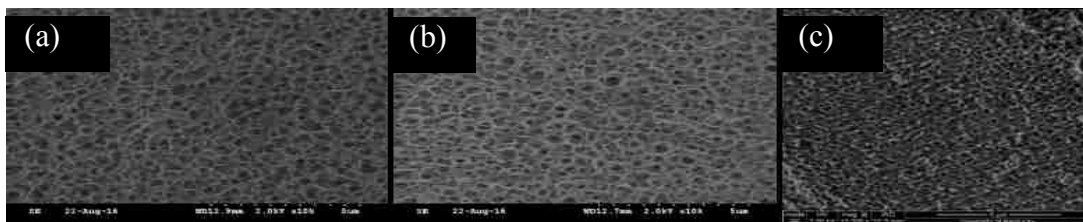


Figure 5.7: SEM imaging of (a) 18%CA, (b) ^PAg-NP/CA and (c) ^CAg-NP/CA membranes pores

Using EDX analysis, the silver loading on ^PAg-NP/CA and ^CAg-NP/CA membranes was found to be 0.2 wt.% and 0.6 wt.%, respectively. The presence of silver in both modified membranes is in agreement with XPS analysis (*Table 5.2* (^CAg-NP/CA membranes only)). Physical and chemical attachment of Ag-NPs was due to 0.25 wt.% by polymer and by bath solution respectively. Signs of silver agglomeration were present in the ^PAg-NP/CA (*Fig. 5.8*), where larger clusters of silver were observed. The smaller concentration of silver on the ^PAg-NP/CA was likely due to the casting process.

Ag-NPs were added to the dope solution, so some of the silver was likely within the membrane matrix and not present on the surface. This would also decrease the antimicrobial activity of the Ag-NPs. Conversely, Ag-NPs were covalently bonded directly to the surface of CA/GMA/CYS membranes (as shown in *Fig. 5.3a*) to form ^CAg-NP/CA membranes. Thus, the Ag-NPs were more concentrated on the surface and believed to be more active.

When nanoparticles are mixed with polymeric dope solutions, inconsistent mixing can occur, which can increase NP agglomeration and ultimately decrease efficiency [90, 91]. Even through consistent sonication, agglomeration is difficult to prevent, and this was observed for ^PAg-NP/CA (*Fig. 5.8*). ^CAg-NP/CA membranes displayed a more uniform dispersion of silver on the membrane (*Fig. 5.9*) resulting from the covalent bonding of the Ag-S reactions (*Fig. 5.3b*). The presence of the gold (Au) peak was due to the gold-palladium that was sputtered onto the membranes, which was used to increase conductivity of the membranes. EDX analysis also verified that silver addition was successful.

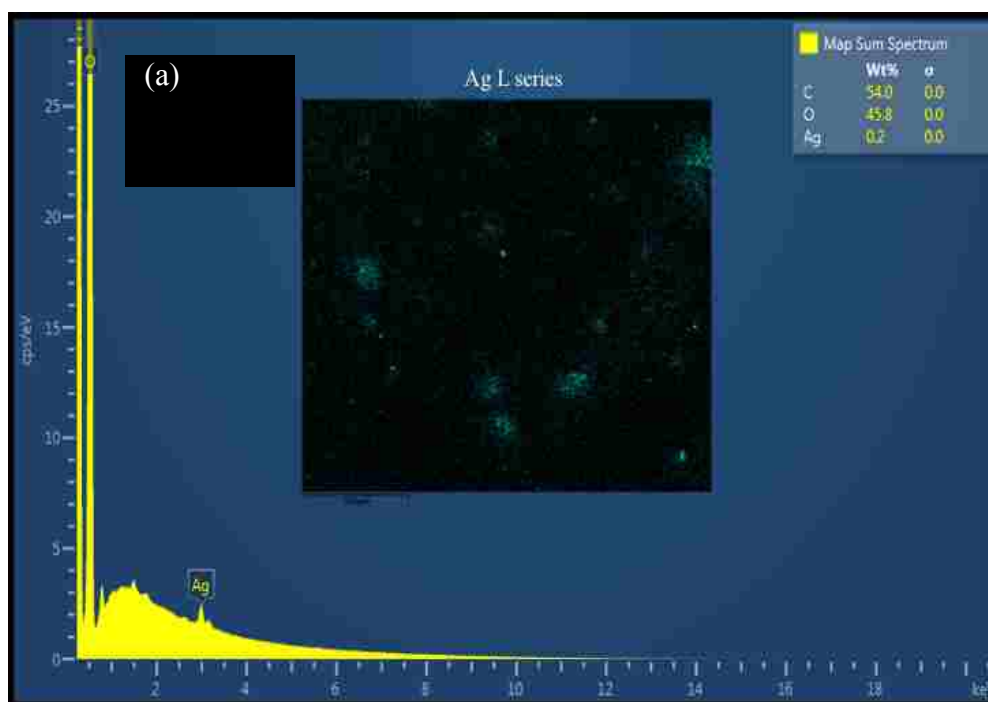


Figure 5.8: EDX mapping analysis of ^PAg-NP/CA membranes

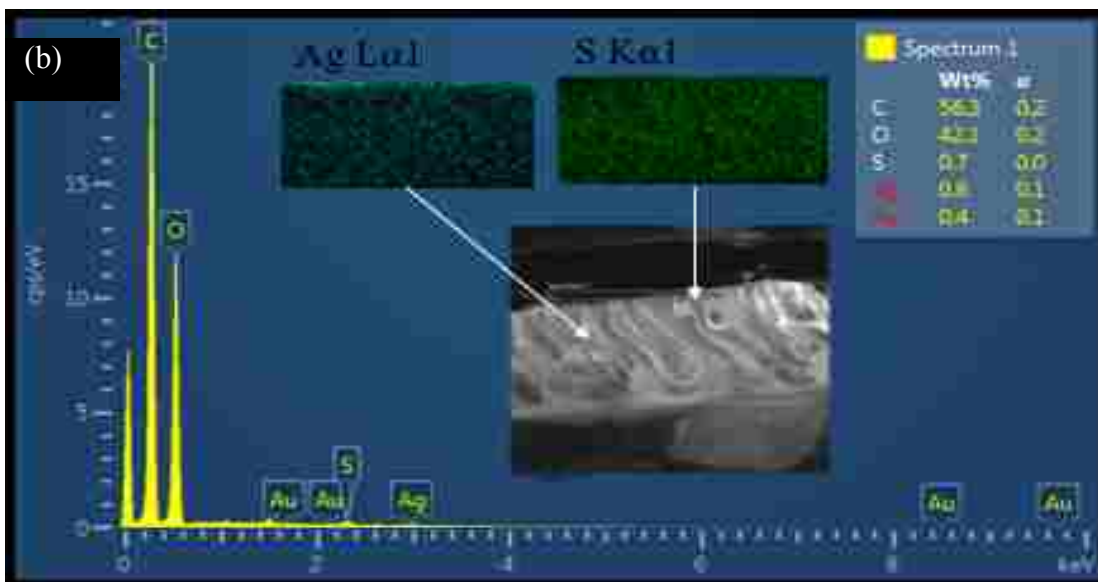


Figure 5.9: EDX mapping analysis of ^CAg-NP/CA membranes

5.3.4 Hydrophilicity of the Membranes

The contact angle of the baseline CA membranes was found to be $59.6 \pm 3.7^\circ$, indicating they were hydrophilic. While membranes cast here showed either slight increases or decreases in contact angle, none of these were statistically different, *Fig. 5.10* [30]. Since acetyl groups have a direct impact on the membranes hydrophilicity [63], it was hypothesized that contact angle increases were due to a reduced concentration of the acetyl groups during the functionalization of the membranes. With the increase in hydrophobicity for ^PAg-NP/CA membranes, permeability was expected to decrease; however, the presence of more pore channels (*Fig. 5.7b*) negated this as it should have a more profound effect.

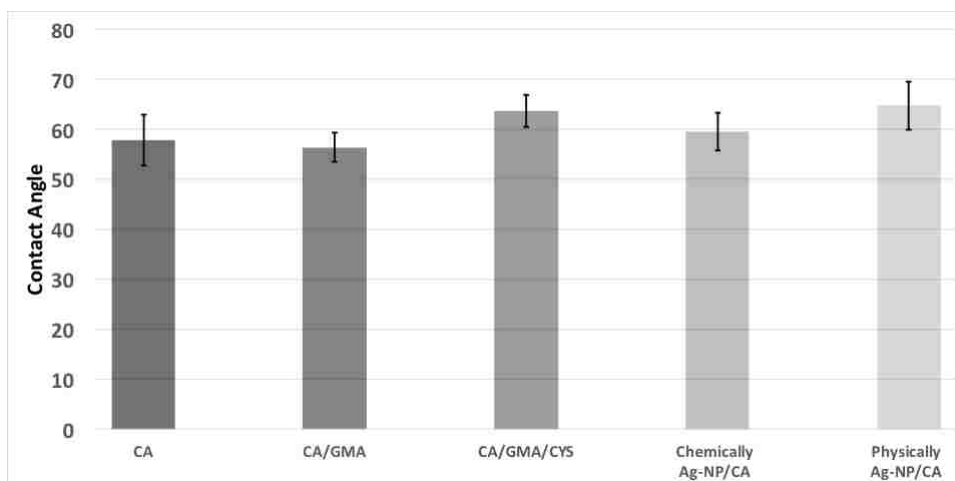


Figure 5.10: Contact angles of virgin and modified CA membranes

5.4 Filtration Experiments

5.4.1 Flux Decline

Permeability studies were performed in dead-end filtration mode on CA, ^PAg-NP/CA and ^CAg-NP/CA membranes at a constant pressure of 4.14 bars (60 psi) with synthetic brackish water containing 10⁴ CFU/mL *Pseudomonas fluorescens*, Fig. 5.11. All experiments were performed to filter the same volume of feed solution; hence, filtration times varied from approximately 6 hours to 14 hours. Experiments were also performed in triplicate and error bars indicate standard deviations. Reverse flow filtrations were performed using DI water to remove reversible fouling in order to recover the initial flux from the start of the filtrations.

Table 5.3 summarizes initial, final and recovered flux values for each membrane, which had thickness averaging 115-135 μm. ^PAg-NP/CA membranes displayed higher flux values during filtration, which might have been caused by the presence of more pore channels due to the pore-forming effect of Ag-NPs, as shown in Fig. 5.6b [90, 91]. ^CAg-NP/CA membranes represented the lowest flux (Table 5.3), which may be due to more crosslinking present in the membranes due to the subsequent reactions leading to the chemical attachment of the Ag-NPs, especially the homopolymerization of GMA and CA [15]. With more crosslinking present in the membrane's morphology, it was possible the pore channels were more irregular than the CA membranes, causing a shift in flow. This hypothesis was supported by SEM imaging since ^CAg-NP/CA membranes (Fig. 5.7c) displayed tighter pore networks as compared to those of CA membranes (Fig. 5.7a).

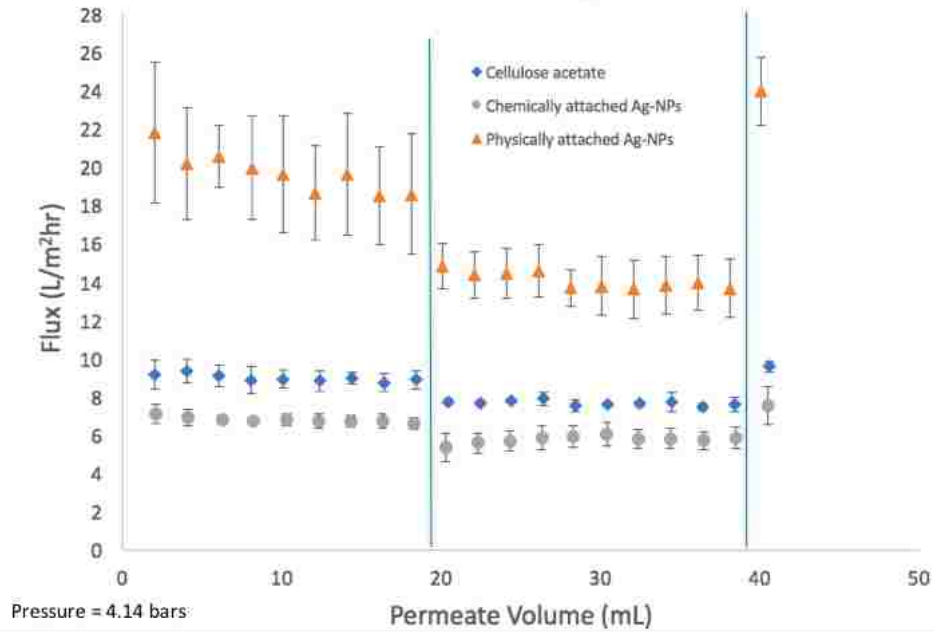
Table 5.3: Flux values obtained from dead-end filtration

Membranes	Initial flux (L/m ² hr)	Final flux (L/m ² hr)	Flux recovery (L/m ² hr)	Flux decline (%)
CA	9.1±0.7	7.6±0.4	9.5±0.3	16.4±8.4
^P Ag-NP/CA	21.7±3.7	13.6±1.5	23.9±1.8	35.9±14.0
^C Ag-NP/CA	7.1±0.5	5.8±0.6	7.5±1.0	17.6±5.2

Filtration studies, shown in Figures 5.11, show fouling occurred, as observed by flux declines during filtration of brackish water containing 10⁴ CFU/mL cells. ^PAg-

NP/CA membranes had the highest average flux decline percentage ($35.9\% \pm 14.0\%$), while $^C\text{Ag-NP/CA}$ and $^P\text{Ag-NP/CA}$ membranes showed lower average flux declines of $16.4\% \pm 8.4\%$ and $17.6\% \pm 5.2\%$, respectively (*Table 5.3*). The flux decline of the membranes was likely due from the accumulation of live bacteria for CA membrane filtration and dead bacteria for $^C\text{Ag-NP/CA}$ membrane filtration. No biofilm formation was expected since not enough time (6-14 hours) nor additional nutrients were provided. Additional long-term biofouling studies were performed to verify the low-biofouling potential of the membranes, and are discussed in *Section 5.5*. The high flux decline of the $^P\text{Ag-NP/CA}$ membranes ($35.9\% \pm 14.0\%$) showed the membranes were more susceptible to fouling than both CA and $^C\text{Ag-NP/CA}$ membranes. Agglomerated Ag-NPs present on the $^P\text{Ag-NP/CA}$ membranes (*Fig. 5.8b*) may have detached during filtration and have concentrated on the surface, which is in agreement with literature studies that have shown that approximately 95% of Ag-NPs had the potential to leach from membranes [96]. Furthermore, SEM and EDX images, shown in *Fig. 5.6* and *Fig. 5.8b*, showed agglomerated Ag-NPs on the surface of $^P\text{Ag-NP/CA}$ membranes. Thus, it was believed that the flux decline was caused by increased resistance of fouling cause by the Ag-NPs present on the membrane surfaces [8] and an accumulation of bacteria on the membrane.

CA membranes displayed an average flux recovery of $108\% \pm 9\%$, while $^P\text{Ag-NP/CA}$ membranes showed $127\% \pm 11\%$ and $^C\text{Ag-NP/CA}$ membranes $112\% \pm 14\%$. These higher obtained flux values over the initial flux might have been due to permanent membrane damage from the physical cleaning (i.e., reverse flow) and from the creation of macrovoids in the pores during the reverse flow. It was also possible that agglomerated Ag-NPs might have detached from the membranes to create larger macrovoids leading to the higher flux recovery observed with $^P\text{Ag-NP/CA}$ membranes. Overall, these numbers suggest that no irreversible fouling was present.



Figures 5.11: Filtration of CA, ^CAg-NP/CA and ^PAg-NP/CA membranes all performed at 4.14 bars (60 psi)

5.4.2 Salt Rejection

Overall, low salt rejection was achieved by all membranes (*Table 5.4*), which was expected due to the larger pores of UF membranes (typically 5-20 nm) [46]. CA and ^PAg-NP/CA membranes both showed similar rejections while ^CAg-NP/CA membranes resulted in higher salt rejection. As previously discussed, ^CAg-NP/CA membranes were found to possess tighter pores (due to additional crosslinking) and reduced flux decline (*Fig. 5.7* and *Table 5.3*). It was hypothesized that the significant increase of salt rejections in the ^CAg-NP/CA membranes were due to the tighter pores.

Table 5.4: Salt rejections of CA, ^PAg-NP/CA and ^CAg-NP/CA membranes

Membranes	Salt rejection (%)
CA	12.4±3.5
^P Ag-NP/CA	17.6±4.0
^C Ag-NP/CA	32.4±3.9

5.4.3 Silver Leaching Crossflow Studies

In order to study the strength of Ag-NP immobilization on and the possible leaching of silver from the ^PAg-NP/CA and ^CAg-NP/CA membranes, long-term crossflow filtration studies were performed. If the membranes were to continuously

leach silver, they would eventually lose their antimicrobial properties [37], and previous studies showed that up to 95% of Ag-NPs had the potential to leach from CA membranes at room temperature [96]. Table 5.5 summarizes results from leaching studies, and shows that after 7 days of continuous filtration more silver leached from ^PAg-NP/CA membranes (146±54 ppb) as compared to ^CAg-NP/CA membranes (37±19 ppb). Three different membrane samples from different fabricated sheets were used for each crossflow filtration, which may explain the high standard deviations.

It was hypothesized that through physical attachment, the Ag-NPs were more likely to leach from the membranes because they were only entrapped in the matrix of the membrane and its pores. For Ag-NPs that were chemically attached, it was expected the leaching would be lower. Since ^CAg-NP/CA membranes were made via immersion of solvent, it was possible some Ag-NPs were entrapped in the matrix of the pores, which would correspond to the leaching observed. According to EPA and WHO, the secondary maximum contaminant levels (SMCL) in drinking water for silver ions is 0.1 mg/L or 100 ppb [41]. All leaching studies performed with ^PAg-NP/CA membranes would have failed to comply with these drinking water regulations, while all ^CAg-NP/CA membranes were below drinking water regulations.

Table 5.5: Leached silver from ^PAg-NP/CA and ^CAg-NP/CA membranes over a week

Time (day)	^P Ag-NP/CA membrane (ppb)	^C Ag-NP/CA membrane (ppb)
1	98±66	60±15
2	128±85	54±26
3	134±84	41±28
4	146±71	46±26
5	136±53	42±22
6	156±63	39±20
7	146±54	37±19
8	-	34±17

5.5 Biofouling Studies

5.5.1 Biofouling Experiments

Forty-eight hour controlled filtration experiments were performed to induce increased biofilm formation on test membranes. These biofouling studies were performed in order to further identify the antimicrobial effects of the Ag-NPs when added to the CA membranes. These differed from filtration studies by supplementing the feed water with 30 mg/L sodium acetate to induce microbial growth [98], and by performing filtration under low pressure for 48 hours in dead-end filtration mode at 0.69-1.03 bars (10-15 psi).

Fluorescence microscopy was performed on live/dead cells present on membrane samples to determine the relative amount of cells that were present in the sample. The stained cells could be seen under the microscope, yet it was difficult to observe all present cells on the sample media because of the focus of the microscope. Furthermore, depth perception of the cells was a challenge because of free-floating bacteria in the samples. Prior to filtration, all experiments had 10^4 cells/mL in the feed solution. After 48 hours, there was a drop in the numbers of live cells (*Fig. 5.12a,c,e*, for CA, ^PAg-NP/CA and ^CAg-NP/CA, respectively) and dead cells (*Fig. 5.12b,d,f*, for CA, ^PAg-NP/CA and ^CAg-NP/CA, respectively) present when membranes with Ag-NPs were used, as expected. There was a reasonable drop in live cells from the CA membranes (*Fig. 5.12a*) to the ^PAg-NP/CA (*Fig. 5.12c*), and ^CAg-NP/CA (*Fig. 5.12e*) membranes, which was hypothesized to be caused by the Ag-NPs antimicrobial properties. Based on the previous EDX analysis of the ^CAg-NP/CA membranes (*Fig. 5.9*), a more uniformed distribution of silver could lead to more interactions with bacteria that happened to have come in contact with the membrane during the 48-hour filtration study [33]. The decrease in dead cell counts when using modified membranes could have been due to the prevention of bacterial replication (i.e. growth), cellular lysis [116] and inactivation of important cell enzymes that participate in nutrient acquisition [37] and NADH [35] in the presence of Ag-NPs [35, 37, 85].

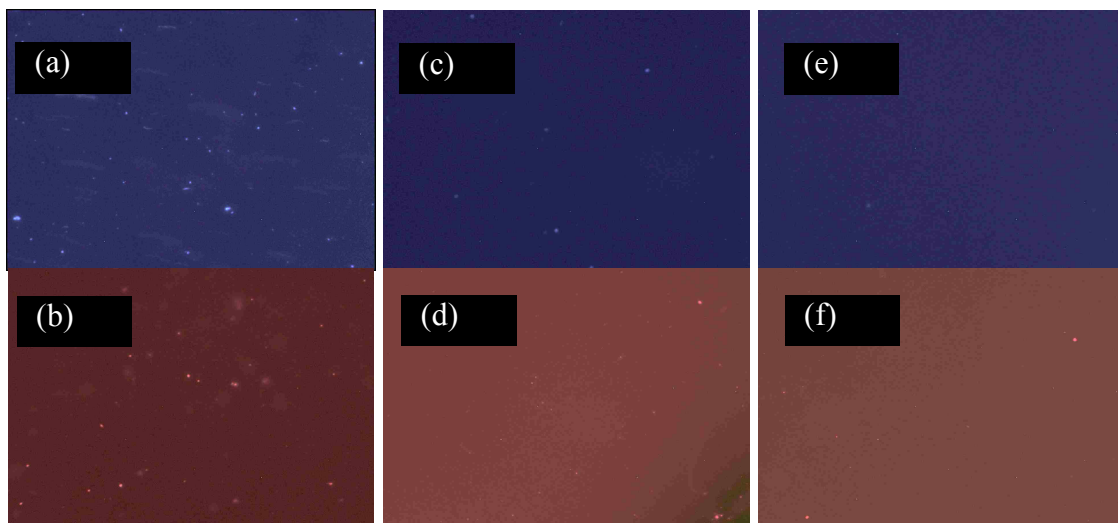


Figure 5.12: Fluorescence microscopy images of live/dead cells detached from (a-b) CA, (c-d) $^P\text{Ag-NP/CA}$, and (e-f) $^C\text{Ag-NP/CA}$ membranes respectively (All images were brightened to create better contrast of the images for easier observation).

Location of the silver on the membranes would impact the antimicrobial effects. It was hypothesized that since $^P\text{Ag-NP/CA}$ membranes (*Fig. 5.13b*) had more silver aggregation and less uniformed distribution of silver, there would be less surface interactions with bacteria. EDX mapping analysis showed there was more uniformed distribution of silver in the $^C\text{Ag-NP/CA}$ membranes (*Fig. 5.9*), which suggested more possible interactions between bacterial cells and silver. It appeared that $^C\text{Ag-NP/CA}$ membranes had a stronger antimicrobial effect towards bacteria than the physical attachment of silver, but more biological studies are needed on the biocidal effects of Ag-NPs.

Based on biofouling results, CA membranes flux decline was hypothesized to be caused by the accumulation of live cells on the membrane and the start of biofouling (*Fig. 5.13a*), while it was likely $^C\text{Ag-NP/CA}$ membranes flux decline was due to accumulation of dead cells on the surface of the membranes, which agrees with the observed presence of dead cells on $^C\text{Ag-NP/CA}$ membranes (*Figure 5.12f*). It is important to note that flux decline studies were performed in shorter periods of time, so only bacterial cells would accumulate on the membranes. The higher flux decline of $^P\text{Ag-NP/CA}$ membranes was likely due agglomerated Ag-NPs present on membrane surfaces (*Fig. 5.8*) that were not immobilized and thus detached from the membrane to accumulate

on the membrane surfaces. With chemically attached NPs, silver nanoparticles were more immobilized (*Table 5.5*), more widely dispersed (*Fig. 5.9*), contributed to higher salt rejections (*Table 5.4*) and proposed better antimicrobial properties (*Fig. 5.12 a-f*) for the ^CAg-NP/CA membranes.

6 CONCLUSIONS AND RECOMMENDATIONS

6.1 Conclusions

The overarching goal of this work was to develop a method to chemically attach casein-coated Ag-NPs to CA membranes to produce low-biofouling membranes that would not leach nanoparticles for potential pretreatment processes. To this end, CA was homopolymerized with poly-GMA and functionalized with cysteamine for its thiol groups in order to covalently attach Ag-NPs to the membrane surface (^CAg-NP/CA membranes). Membranes were characterized through structural, morphological, permeation and biofouling studies. XPS and EDX elemental analysis showed the Ag-NPs were successfully attached and dispersed uniformly across the membrane surfaces. Addition of silver nanoparticles did not affect membrane hydrophilicity. To evaluate improvements, comparisons between CA membranes and membranes with physically and chemically attached Ag-NPs were studied.

Membranes with Ag-NPs physically blended (^PAg-NP/CA) displayed more pore channels in their cross-sections, and exhibited higher average flux values likely due to the Ag-NPs acting as pore formers during the phase-inversion process. These membranes also had the highest average flux decline during short-term filtration studies, which was hypothesized to be caused by the accumulation of both detached Ag-NPs and bacteria on the membrane surface. There was little difference in pore channel morphology between CA and ^CAg-NP/CA membranes, but the latter displayed a tighter pore network compared to the other membranes due to GMA crosslinking, which contributed to its lower average flux. While the ^CAg-NP/CA membranes had a similar average flux decline compared to the CA membranes, the chemically attached Ag-NPs expressed the highest salt rejections. Lastly, ^CAg-NP/CA membranes appeared to better control biofouling as compared to CA membranes, based on the reduction in the amount of cells on the membrane surface when under induced biofilm formation conditions. Therefore, immobilizing Ag-NPs onto membrane surfaces allowed a more uniform dispersion of NPs, which in turn led to more surface interactions with bacteria, and therefore, better antimicrobial properties. There was minimum leaching of silver during cross-flow filtration of ^CAg-NP/CA membranes, and the leached water could still meet drinking

water regulations. With widely dispersed immobilized Ag-NPs, these membranes possessed better antimicrobial properties and salt rejections than conventional membranes or membranes blended with Ag-NPs. While a novel method to embed membranes with Ag-NPs with minimal leaching of the nanoparticles was developed here, additional studies are still needed to fully understand the anti-microbial properties of the membranes.

6.2 Recommendations

The chemical attachment of Ag-NPs to CA membranes was successfully performed, and the resulting ^CAg-NP/CA membranes showed reduced biofouling behavior. Therefore, additional studies should be performed to further improve their characteristics, including the following suggestions:

- Modify amounts of reagents and solvent used to perform the chemical attachment of Ag-NPs to improve its performance and to determine best concentration for maximum surface coverage.
- Find green, economical and less hazardous alternatives to using DMSO solvent and cysteamine reagent, as both are costly and hazardous.
- Conduct silver leaching studies with varying pH levels, solutions and time to better understand its behaviors in the presence of NOMs and monovalent/divalent ions.
- Perform longer fouling experiments under cross-flow filtration to better understand silver effects on biofilms.
- Gain better quantitative/qualitative data regarding to live/dead cell counts and biofilm formation.
- Determine the rate of cellular attachment on CA and physically/chemically attached Ag-NPs during biofouling experiments.
- Continuously run filtration experiments after first reverse flow to better understand flux decline and recovery of membranes over a period of time. This would provide a better idea on the durability on the membranes.

- Develop better methods to attach the Ag-NPs onto CA membranes, such as electrospinning, copolymerization of polymers, carbamate chemistry and thiol-bromo click reactions.
- Perform atomic force microscopy to determine membrane surface roughness in order to better explain the fouling process.
- Perform Fourier transform infrared spectroscopy on membrane surfaces in order to determine if any cells remain by the presence of phosphates.
- Perform plate counting of the biofouled membranes after induced increased biofilm formation experiments to determine approximate cell counts.

APPENDIX

List of Abbreviations

• BPO	-----	benzoyl peroxide
• CA	-----	cellulose acetate
• CYS	-----	cysteamine
• DMF	-----	N,N-dimethylformamide
• DMSO	-----	dimethyl sulfoxide
• EDX	-----	Energy-dispersive X-ray spectroscopy
• EPA	-----	Environmental Protection Agency
• EPS	-----	extracellular polymeric substance
• FTIR	-----	Fourier transform infrared spectroscopy
• HCl	-----	hydrochloric acid
• GMA	-----	glycidyl methacrylate
• ICP-OES	-----	Inductively coupled plasma optical emission spectroscopy
• MF	-----	microfiltration
• Mono-GMA	-----	monomer glycidyl methacrylate
• MRSA	-----	methicillin-resistant <i>S. epidermidis</i>
• NF	-----	nanofiltration
• NMP	-----	N-methyl-2-pyrrolidone
• NOM	-----	natural organic matter
• NP	-----	nanoparticle
• TFC	-----	thin-film composite
• PA	-----	polyamide
• PAN	-----	polyacrylonitrile
• PANCMA	-----	poly(acrylonitrile-comaleic acid)
• PEG	-----	polyethylene glycol
• PES	-----	polyethersulfone
• PI	-----	polyimide
• Poly-GMA	-----	polymerized glycidyl methacrylate
• PP	-----	polypropylene
• PSf	-----	polysulfone
• PTFE	-----	poly(tetrafluoroethylene)
• PVA	-----	polyvinyl alcohol
• PVC	-----	polyvinyl chloride
• PVDF	-----	poly(vinylidene fluoride)
• PVP	-----	polyvinylpyrrolidone
• RO	-----	reverse osmosis
• ROS	-----	reactive oxidative species
• SEM	-----	Scanning electron microscope
• SMCL	-----	secondary maximum contaminant levels
• TEM	-----	Transmission electron microscope

- UF ----- ultrafiltration
- UV ----- ultraviolet
- UV/Vis ----- Ultraviolet-visible spectroscopy
- WHO ----- World Health Organization
- XPS ----- X-ray photoelectron spectroscopy

APPENDIX B

Data

Table B.1: Flux data for CA membranes with DI water, and 10⁴ CFU/mL / brackish water

Cellulose Acetate												
Date	Time	Run	volume (in mL)	volume (in L)	pressure (psi)	hours	minutes	seconds	total time (hr)	cumulative total time (hr)	flux L/(m ² *hr)	Normalized
Precompaction												
7/25/16	11:44am	1	2	0.002	60		25	59	0.433	0.433		
-	12:20pm	2	2	0.002	60		28	34	0.476	0.00	9.33	1.000
-	1:20pm	3	2	0.002	60		27	36	0.460	0.46	9.66	1.035
-	1:53pm	4	2	0.002	60		28	36	0.477	0.94	9.32	0.999
-	2:23pm	5	2	0.002	60		29	9	0.486	1.42	9.15	0.980
-	2:54pm	6	2	0.002	60		29	34	0.493	1.92	9.02	0.966
-	3:25pm	7	2	0.002	60		29	30	0.492	2.41	9.04	0.968
-	3:55pm	8	2	0.002	60		29	32	0.492	2.90	9.03	0.967
-	4:25pm	9	2	0.002	60		29	38	0.494	3.39	9.00	0.964
-	5:00pm	10	2	0.002	60		29	37	0.494	3.89	9.00	0.965
Brackish water												
7/27/16	9:35am	1	2	0.002	60		34	25	0.574	4.46	7.75	0.830
-	10:15am	2	2	0.002	60		34	32	0.576	5.04	7.72	0.827
-	10:52am	3	2	0.002	60		34	31	0.575	5.61	7.73	0.828
-	11:29am	4	2	0.002	60		32	16	0.538	6.15	8.26	0.885
-	12:30pm	5	2	0.002	60		34	4	0.568	6.72	7.83	0.839
-	12:40pm	6	2	0.002	60		34	52	0.581	7.30	7.65	0.819
-	1:29pm	7	2	0.002	60		34	56	0.582	7.88	7.63	0.818
-	2:06pm	8	2.05	0.0021	60		32	58	0.549	8.43	8.29	0.888
-	2:44pm	9	2	0.002	60		34	52	0.581	9.01	7.65	0.819
-	3:22pm	10	2	0.002	60		33	33	0.559	9.57	7.95	0.851
Backwash												
		1		0	30	1			1			
Flux recovery		1	2	0.002	60		28	3	0.4675	10.04	9.51	1.018

Table B.2: Flux data for CA membranes with DI water, and 10⁴ CFU/mL / brackish water

Cellulose acetate												
Date	Time	Run	volume (in mL)	volume (in L)	pressure (psi)	hours	minutes	seconds	total time (hr)	cumulative total time (hr)	flux L/(m ² *hr)	Normalized
Precompaction												
7/28/16	9:54am	1	2	0.002	60		24	17	0.405	0.40		
-	10:21am	2	2	0.002	60		27	28	0.458	0.00	9.71	1.000
-	10:47am	3	2	0.002	60		27	32	0.459	0.46	9.69	0.998
-	11:16am	4	2	0.002	60		28	11	0.470	0.93	9.46	0.975
-	11:46am	5	2	0.002	60		28	33	0.476	1.40	9.34	0.962
-	12:15pm	6	2	0.002	60		28	37	0.477	1.88	9.32	0.960
-	12:44pm	7	3.12	0.0031	60		45	20	0.756	2.64	9.18	0.945
-	1:33pm	8	2	0.002	60		29	4	0.484	3.12	9.17	0.945
-	2:02pm	9	2	0.002	60		29	34	0.493	3.61	9.02	0.929
-	2:34pm	10	2	0.002	60		28	57	0.483	4.10	9.21	0.949
Brackish water												
7/29/16	9:22am	1	2	0.002	60		35	10	0.586	4.68	7.58	0.781
-	10:00am	2	2.05	0.0021	60		36	25	0.607	5.29	7.51	0.773
-	10:38am	3	2	0.002	60		34	44	0.579	5.87	7.68	0.791
-	11:15am	4	2	0.002	60		35	6	0.585	6.45	7.60	0.783
-	11:52am	5	2	0.002	60		35	26	0.591	7.04	7.53	0.775
-	12:30pm	6	2	0.002	60		35	1	0.584	7.63	7.62	0.784
-	1:06pm	7	2	0.002	60		35	44	0.596	8.22	7.46	0.769
-	1:44pm	8	2	0.002	60		36	6	0.602	8.83	7.39	0.761
-	2:20pm	9	2	0.002	60		36	45	0.613	9.44	7.26	0.747
-	3:05pm	10	2	0.002	60		36	51	0.614	10.05	7.24	0.745
Backwash												
		1		0	30	1			1.000			
Flux recovery		1	2.34	0.0023	60		31	42	0.528	10.64	9.84	0.956

Table B.3: Flux data for CA membranes with DI water, and 10⁴ CFU/mL / brackish water

Cellulose acetate												
Date	Time	Run	volume (in mL)	volume (in L)	pressure (psi)	hours	minutes	seconds	total time (hr)	cumulative total time (hr)	flux L/(m ² *hr)	Normalized
Precompaction												
8/10/16	9:02am	1	2	0.002	60		29	51	0.498	0.50		
-	9:33am	2	2.05	0.0021	60		33	1	0.550	0.00	8.28	1.000
-	10:20am	3	2	0.002	60		30	58	0.516	0.52	8.61	1.040
-	-	4	2	0.002	60		31	41	0.528	1.04	8.42	1.017
-	-	5	2	0.002	60		33	10	0.553	1.60	8.04	0.971
-	11:57am	6	2	0.002	60		31	51	0.531	2.13	8.37	1.011
-	1:38pm	7	2	0.002	60		32	40	0.544	2.67	8.16	0.986
-	2:10pm	8	2	0.002	60		31	8	0.519	3.19	8.57	1.035
-	2:44pm	9	2	0.002	60		32	41	0.545	3.74	8.16	0.986
-	3:21pm	10	2	0.002	60		31	58	0.533	4.27	8.34	1.008
Brackish water												
8/11/16	8:56am	1	2	0.002	60		33	57	0.566	4.83	7.85	0.949
-	9:32am	2	2	0.002	60		34	20	0.572	5.41	7.77	0.938
-	10:11am	3	2	0.002	60		33	40	0.561	5.97	7.92	0.957
-	-	4	2	0.002	60		34	30	0.575	6.54	7.73	0.934
-	-	5	2	0.002	60		37	8	0.619	7.16	7.18	0.867
-	-	6	2	0.002	60		35	48	0.597	7.76	7.45	0.900
-	-	7	2	0.002	60		34	21	0.573	8.33	7.76	0.938
-	1:21pm	8	2	0.002	60		35	37	0.594	8.92	7.49	0.904
-	2:05pm	9	2	0.002	60		35	42	0.595	9.52	7.47	0.902
-	2:42pm	10	2	0.002	60		35	20	0.589	10.11	7.55	0.912
Backwash												
		1		0	30	1			1.000			
Flux recovery		1	2.34	0.0023	60		31	42	0.528	10.64	9.84	1.189

Table B.4: Flux data for ^PAg-NP/CA membranes with DI water, and 10⁴ CFU/mL / brackish water

Physically attached Ag-NPs												
Date	Time	Run	volume (in mL)	volume (in L)	pressure (psi)	hours	minutes	seconds	total time (hr)	cumulative total time (hr)	flux L/(m ² *hr)	Normalized
Precompaction												
1/20/17	9:28am	1	2	0.002	60		12	40	0.211	0.21		
-	9:45am	2	2	0.002	60		16	10	0.269	0.00	16.49	1.000
-	9:59am	3	2	0.002	60		12	8	0.202	0.20	21.98	1.332
-	10:12am	4	2	0.002	60		12	56	0.216	0.42	20.62	1.250
-	10:26am	5	2	0.002	60		13	26	0.224	0.64	19.85	1.203
-	2:00pm	6	2	0.002	60		12	20	0.206	0.85	21.62	1.311
-	2:12pm	7	2	0.002	60		13	38	0.227	1.07	19.56	1.186
-	2:27pm	8	2	0.002	60		11	51	0.198	1.27	22.50	1.364
-	2:41pm	9	2	0.002	60		12	45	0.213	1.48	20.92	1.268
-	2:56pm	10	2	0.002	60		13	17	0.221	1.71	20.08	1.217
Brackish water												
1/22/17	9:31am	1	2	0.002	60		18	3	0.301	2.01	14.77	0.896
-	9:56am	2	2	0.002	60		18	34	0.309	2.32	14.36	0.871
-	10:15am	3	2	0.002	60		18	47	0.313	2.63	14.20	0.861
-	10:35am	4	2	0.002	60		18	25	0.307	2.94	14.48	0.878
-	10:57am	5	2	0.002	60		19	43	0.329	3.26	13.52	0.820
-	11:17am	6	2	0.002	60		19	14	0.321	3.59	13.86	0.841
-	11:38am	7	2	0.002	60		19	13	0.320	3.91	13.88	0.841
-	11:59am	8	2	0.002	60		19	46	0.329	4.24	13.49	0.818
-	12:21pm	9	2	0.002	60		19	4	0.318	4.55	13.99	0.848
-	1:01pm	10	2	0.002	60		19	17	0.321	4.87	13.83	0.838
Backwash												
		1		0	30	1			1.000			
Flux recovery		1	2	0.002	60		10	34	0.176	5.05	25.24	1.530

Table B.5: Flux data for ^PAg-NP/CA membranes with DI water, and 10⁴ CFU/mL / brackish water

Physically Attached Ag-NPs												
Date	Time	Run	volume (in mL)	volume (in L)	pressure (psi)	hours	minutes	seconds	total time (hr)	cumulative total time (hr)	flux L/(m ² *hr)	Normalized
Precompaction												
1/25/17	10:48am	1	2	0.002	60		8	37	0.14	0.144		
-	11:00am	2	2	0.002	60		10	58	0.18	0.000	24.32	1.000
-	11:13am	3	2	0.002	60		12	1	0.20	0.200	22.19	0.913
-	11:27am	4	2	0.002	60		13	6	0.22	0.419	20.36	0.837
-	11:41am	5	2	0.002	60		11	47	0.20	0.615	22.63	0.931
-	11:54am	6	2	0.002	60		12	19	0.21	0.820	21.65	0.890
-	12:08pm	7	2	0.002	60		12	46	0.21	1.033	20.89	0.859
-	12:22pm	8	2	0.002	60		12	48	0.21	1.246	20.83	0.857
-	12:36pm	9	2	0.002	60		14	3	0.23	1.481	18.98	0.781
-	12:50pm	10	2	0.002	60		12	17	0.20	1.685	21.71	0.893
Brackish water												
1/27/17	9:35am	1	2	0.002	60		16	26	0.27	1.959	16.23	0.667
-	9:54am	2	2	0.002	60		16	50	0.28	2.240	15.84	0.651
-	10:12am	3	2	0.002	60		16	41	0.28	2.518	15.98	0.657
-	10:31am	4	2	0.002	60		16	36	0.28	2.794	16.06	0.661
-	10:50am	5	2	0.002	60		18	2	0.30	3.095	14.79	0.608
-	11:09am	6	2	0.002	60		16	51	0.28	3.376	15.83	0.651
-	11:28am	7	2	0.002	60		17	6	0.29	3.661	15.59	0.641
-	11:48am	8	2	0.002	60		17	15	0.29	3.948	15.46	0.636
-	12:07pm	9	2	0.002	60		16	45	0.28	4.228	15.92	0.655
-	12:26pm	10	2	0.002	60		17	5	0.28	4.512	15.61	0.642
Backwash		1		0	30	1			1.00			
Flux recovery		1	2	0.002	60		10	41	0.18	4.690	24.96	1.027

Table B.6: Flux data for ^PAg-NP/CA membranes with DI water, and 10⁴ CFU/mL / brackish water

Physically Attached Ag-NPs												
Date	Time	Run	volume (in mL)	volume (in L)	pressure (psi)	hours	minutes	seconds	total time (hr)	cumulative total time (hr)	flux L/(m ² *hr)	Normalized
Precompaction												
1/30/17	9:52am	1	2	0.002	60		8	11	0.136	0.14		
-	10:03am	2	2	0.002	60		10	57	0.183	0.00	24.35	1.000
-	10:17am	3	2	0.002	60		12	59	0.216	0.22	20.54	0.843
-	10:30am	4	2	0.002	60		11	50	0.197	0.41	22.54	0.925
-	10:43am	5	2	0.002	60		12	42	0.212	0.63	21.00	0.862
-	10:57am	6	2	0.002	60		13	25	0.224	0.85	19.88	0.816
-	12:29pm	7	2	0.002	60		14	10	0.236	1.09	18.82	0.773
-	2:28pm	8	2	0.002	60		13	20	0.222	1.31	20.00	0.821
-	2:40pm	9	2	0.002	60		13	57	0.233	1.54	19.12	0.785
-	2:59pm	10	2	0.002	60		14	50	0.247	1.79	17.98	0.738
Brackish water												
1/31/17	9:14am	1	2	0.002	60		17	56	0.299	2.09	14.87	0.611
-	9:34am	2	2	0.002	60		18	34	0.309	2.40	14.36	0.590
-	9:55am	3	2	0.002	60		18	11	0.303	2.70	14.67	0.602
-	10:14am	4	2	0.002	60		17	51	0.298	3.00	14.94	0.613
-	-	5	2	0.002	60		19	15	0.321	3.32	13.85	0.569
-	-	6	2	0.002	60		20	19	0.339	3.66	13.13	0.539
-	-	7	2	0.002	60		20	52	0.348	4.00	12.78	0.525
-	-	8	2	0.002	60		18	34	0.309	4.31	14.36	0.590
-	-	9	2	0.002	60		20	7	0.335	4.65	13.26	0.544
-	-	10	2	0.002	60		20	18	0.338	4.99	13.14	0.539
Backwash		1		0	30	1			1.000			
Flux recovery		1	2	0.002	60		11	3	0.184	5.17	24.13	0.991

Table B.7: Flux data for ^PAg-NP/CA membranes with DI water, and 10⁴ CFU/mL / brackish water

Physically attached Ag-NPs												
Date	Time	Run	volume (in mL)	volume (in L)	pressure (psi)	hours	minutes	seconds	total time (hr)	cumulative total time (hr)	flux L/(m ² *hr)	Normalized
Precompaction												
2/13/17	2:58pm	1	2	0.002	60		7	38	0.127	0.13		
-	3:11pm	2	2	0.002	60		12	10	0.203	0.00	21.92	1.000
-	3:30pm	3	2	0.002	60		16	47	0.280	0.28	15.89	0.725
-	3:50pm	4	2.2	0.0022	60		15	47	0.263	0.54	18.59	0.848
-	4:09pm	5	2.1	0.0021	60		17	13	0.287	0.83	16.26	0.742
-	4:28pm	6	2	0.002	60		17	35	0.293	1.12	15.17	0.692
-	5:11pm	7	2	0.002	60		17	35	0.293	1.42	15.17	0.692
-	5:30pm	8	2	0.002	60		17	39	0.294	1.71	15.11	0.689
-	5:48pm	9	2	0.002	60		17	58	0.299	2.01	14.84	0.677
-	6:07pm	10	2	0.002	60		18	30	0.308	2.32	14.41	0.658
Brackish water												
2/15/17	10:40am	1	2	0.002	60		20	1	0.334	2.65	13.32	0.608
-	11:02am	2	2	0.002	60		20	43	0.345	3.00	12.87	0.587
-	11:24am	3	2	0.002	60		20	47	0.346	3.34	12.83	0.585
-	11:44am	4	2	0.002	60		20	57	0.349	3.69	12.73	0.581
-	12:10pm	5	2	0.002	60		21	26	0.357	4.05	12.44	0.568
-	12:36pm	6	2	0.002	60		21	45	0.363	4.41	12.26	0.559
-	1:01pm	7	2	0.002	60		22	0	0.367	4.78	12.12	0.553
-	1:24pm	8	2	0.002	60		22	20	0.372	5.15	11.94	0.545
-	1:48pm	9	2	0.002	60		21	10	0.353	5.50	12.60	0.575
-	2:12pm	10	2	0.002	60		22	18	0.372	5.88	11.96	0.546
Backwash		1		0	30	1			1.000			
Flux recovery		1	2	0.002	60		12	28	0.208	6.08	21.39	0.976

Table B.8: Flux data for ^CAg-NP/CA membranes with DI water, and 10⁴ CFU/mL / brackish water

Chemically attached Ag-NPs												
Date	Time	Run	volume (in mL)	volume (in L)	pressure (psi)	hours	minutes	seconds	total time (hr)	cumulative total time (hr)	flux L/(m ² *hr)	Normalized
Precompaction												
3/13/17	10:05am	1	2	0.002	60		37	10	0.619	0.62		
-	10:45am	2	2	0.002	60		40	25	0.674	0.00	6.60	1.000
-	11:30am	3	2	0.002	60		41	50	0.697	0.70	6.37	0.966
-	12:10pm	4	2	0.002	60		40	49	0.680	1.38	6.53	0.990
-	12:55pm	5	2	0.002	60		41	5	0.685	2.06	6.49	0.984
-	2:05pm	6	2	0.002	60		41	29	0.691	2.75	6.43	0.974
-	2:52pm	7	2	0.002	60		42	7	0.702	3.46	6.33	0.960
-	3:35pm	8	2	0.002	60		41	35	0.693	4.15	6.41	0.972
-	4:20pm	9	2	0.002	60		41	20	0.689	4.84	6.45	0.978
-	5:02pm	10	2	0.002	60		41	39	0.694	5.53	6.40	0.970
Brackish water												
3/14/17	8:52am	1	2	0.002	60		53	29	0.891	6.42	4.99	0.756
-	9:46am	2	2	0.002	60		50	54	0.848	7.27	5.24	0.794
-	10:40am	3	2	0.002	60		51	5	0.851	8.12	5.22	0.791
-	11:35am	4	2	0.002	60		51	51	0.864	8.99	5.14	0.779
-	12:26pm	5	2	0.002	60		50	49	0.847	9.83	5.25	0.795
-	1:24pm	6	2.1	0.0021	60		52	27	0.874	10.71	5.34	0.809
-	2:16pm	7	2	0.002	60		50	53	0.848	11.56	5.24	0.794
-	3:12pm	8	2	0.002	60		51	31	0.859	12.41	5.18	0.785
-	4:06pm	9	2	0.002	60		51	4	0.851	13.27	5.22	0.791
-	5:00pm	10	2	0.002	60		51	17	0.855	14.12	5.20	0.788
Backwash		1		0	30	1			1.000			
Flux recovery		1	2	0.002	60		41	22	0.689	14.81	6.45	0.977

Table B.9: Flux data for ^CAg-NP/CA membranes with DI water, and 10⁴ CFU/mL / brackish water

Chemically attached Ag-NPs												
Date	Time	Run	volume (in mL)	volume (in L)	pressure (psi)	hours	minutes	seconds	total time (hr)	cumulative total time (hr)	flux L/(m ² *hr)	Normalized
Precompaction												
3/22/17	9:27am	1	2	0.002	60		30	57	0.516	0.52		
-	10:05am	2	2	0.002	60		34	58	0.583	0.00	7.63	1.000
-	10:43am	3	2	0.002	60		36	51	0.614	0.61	7.24	0.949
-	11:22am	4	2.42	0.0024	60		48	0	0.800	1.41	6.72	0.881
-	12:12pm	5	2	0.002	60		39	50	0.664	2.08	6.69	0.878
-	12:59pm	6	2.2	0.0022	60		43	23	0.723	2.80	6.76	0.887
-	1:40pm	7	2	0.002	60		39	59	0.666	3.47	6.67	0.875
-	2:55pm	8	2	0.002	60		39	30	0.658	4.13	6.75	0.885
-	3:40pm	9	2	0.002	60		40	56	0.682	4.81	6.51	0.854
-	4:30pm	10	2	0.002	60		41	50	0.697	5.51	6.37	0.836
Brackish water												
3/23/17	-	1	2	0.002	60		55	25	0.924	6.43	4.81	0.631
-	-	2	2	0.002	60		50	44	0.846	7.27	5.26	0.689
-	-	3	2	0.002	60		48	10	0.803	8.08	5.54	0.726
-	-	4	2	0.002	60		43	10	0.719	8.80	6.18	0.810
-	-	5	2	0.002	60		42	51	0.714	9.51	6.22	0.816
-	-	6	2.1	0.0021	60		44	42	0.745	10.26	6.26	0.821
-	-	7	2	0.002	60		44	52	0.748	11.00	5.94	0.779
-	-	8	2	0.002	60		44	36	0.743	11.75	5.98	0.784
-	-	9	2	0.002	60		47	16	0.788	12.53	5.64	0.740
-	-	10	2	0.002	60		43	44	0.729	13.26	6.10	0.800
Backwash												
		1		0	30	1			1.000			
Flux recovery		1	2	0.002	60		31	38	0.527	13.79	8.43	1.105

Table B.10: Flux data for ^CAg-NP/CA membranes with DI water, and 10⁴ CFU/mL / brackish water

Chemically Attached Ag-NPs												
Date	Time	Run	volume (in mL)	volume (in L)	pressure (psi)	hours	minutes	seconds	total time (hr)	cumulative total time (hr)	flux L/(m ² *hr)	Normalized
Precompaction												
3/27/17	9:45am	1	2	0.002	60		35	12	0.587	0.59		
-	10:30am	2	2.22	0.0022	60		42	10	0.703	0.00	7.02	1.000
-	11:09am	3	2	0.002	60		38	9	0.636	0.64	6.99	0.996
-	11:49am	4	2	0.002	60		37	58	0.633	1.27	7.02	1.001
-	12:39pm	5	2	0.002	60		38	42	0.645	1.91	6.89	0.982
-	1:18pm	6	2	0.002	60		37	36	0.627	2.54	7.09	1.010
-	2:00pm	7	2	0.002	60		37	31	0.625	3.17	7.11	1.013
-	2:40pm	8	2	0.002	60		37	57	0.633	3.80	7.03	1.001
-	3:18pm	9	2	0.002	60		37	15	0.621	4.42	7.16	1.020
-	4:03pm	10	2	0.002	60		38	32	0.642	5.06	6.92	0.986
Brackish water												
3/28/17	6:37am	1	2	0.002	60		43	6	0.718	5.78	6.19	0.881
-	7:24am	2	2	0.002	60		43	11	0.720	6.50	6.18	0.880
-	8:13am	3	2	0.002	60		42	37	0.710	7.21	6.26	0.891
-	8:56am	4	2	0.002	60		42	47	0.713	7.92	6.23	0.888
-	9:40am	5	2	0.002	60		43	5	0.718	8.64	6.19	0.882
-	10:28am	6	2.1	0.0021	60		42	58	0.716	9.36	6.52	0.928
-	11:14am	7	2	0.002	60		43	9	0.719	10.08	6.18	0.880
-	12:00pm	8	2	0.002	60		43	14	0.721	10.80	6.17	0.879
-	12:54pm	9	2.3	0.0023	60		49	44	0.829	11.63	6.17	0.878
-	1:39pm	10	2	0.002	60		42	58	0.716	12.34	6.21	0.884
Backwash												
		1		0	30	1			1.000			
Flux recovery		1	2	0.002	60		34	50	0.581	12.92	7.66	1.091

Table B.11 Salt rejection data from CA, ^PAg-NP/CA and ^CAg-NP/CA membranes

	Date	Retentate (microS/cm)	Permeate (microS/cm)	Rejection of solutes R(%)
Physical attachment of Ag-NPs	4/17/17	2290	1820	20.52
	4/17/17	2130	1725	19.01
	4/17/17	2120	1844	13.02
	average	2180	1796.33	17.60
	stdev	95.4	62.9	3.97
Chemical attachment of Ag-NPs	4/20/17	2560	1689	34.02
	4/20/17	2630	1710	34.98
	4/23/17	2330	1683	27.77
	average	2506.67	1694	32.42
	stdev	156.95	14.18	3.92
virgin CA	4/21/17	2110	1934	8.34
	4/21/17	2220	1905	14.19
	4/21/17	2070	1766	14.69
	average	2133.33	1868.33	12.42
	stdev	77.67	89.80	3.53

Table B.12: Crossflow silver leaching study for ^PAg-NP/CA membrane

Test 1 Physically Attached Ag-NPs										
sample	Ag 328.068 ppb	Ag 338.289 ppb	For samples 1-10, time was started at 8:40am 1/19/17							
blank	4.068	6.181	date	time reading	day	hours	minutes	total days	total hours	
1	7.849	9.577	1/19/17	8:40am	0	0	0	0.00	0.00	
2	39.621	39.705	1/19/17	8:41pm	0	12	1	0.50	12.02	
3	44.338	44.343	1/20/17	8:38am	0	23	58	1.00	23.97	
4	43.334	42.664	1/20/17	5:57pm	1	9	17	1.39	33.28	
5	57.082	55.723	1/21/17	8:42am	2	0	2	2.00	48.03	
6	67.93	66.455	1/21/17	8:58pm	2	12	18	2.51	60.30	
7	55.334	53.627	1/22/17	8:51am	3	0	11	3.01	72.18	
8	62.412	59.55	1/22/17	2:51pm	3	6	11	3.26	78.18	
9	103.702	101.124	1/23/17	8:42am	4	0	2	4.00	96.03	
10	104.395	99.709	1/23/17	4:55pm	4	8	15	4.34	104.25	

Table B.13: Crossflow silver leaching study for ^PAg-NP/CA membrane

Test 2 Physically Attached Ag-NPs										
sample	Ag 328.068 ppb	Ag 338.289 ppb	For samples 1-13, time was started at 3:25pm 1/27/17							
blank	11.267	12.672	date	time reading	day	hours	minutes	total days	total hours	
1	42.442	41.331	1/27/17	3:25pm	0	0	0	0.00	0.00	
2	76.629	75.128	1/28/17	8:40am	0	17	25	0.73	17.42	
3	104.468	102.325	1/29/17	10:00am	1	18	35	1.77	42.58	
4	105.787	101.721	1/30/17	8:20am	2	16	55	2.70	64.92	
5	106.402	103.81	1/30/17	10:05pm	3	6	40	3.28	78.67	
6	105.377	101.767	1/31/17	8:25am	3	17	0	3.71	89.00	
7	107.131	103.045	1/31/17	4:40pm	4	1	15	4.05	97.25	
8	85.766	83.896	2/1/17	8:15am	4	16	50	4.70	112.83	
9	111.448	109.834	2/1/17	4:35pm	5	1	10	5.05	121.17	
10	73.14	70.904	2/2/17	8:37am	5	17	12	5.72	137.20	
11	106.496	104.272	2/2/17	4:45pm	6	1	20	6.06	145.33	
12	76.778	73.515	2/3/17	8:15am	6	16	50	6.70	160.83	
13	107.657	102.917	2/3/17	2:22pm	6	22	57	6.96	166.95	

Table B.14: Crossflow silver leaching study for ^PAg-NP/CA membrane

Test 3 Physically Attached Ag-NPs										
sample	Ag 328.068 ppb	Ag 338.289 ppb								
For samples 1-11, time was started at 6:00pm 2/17/17										
			date	time reading	day	hours	minutes	total days	total hours	
blank	1.837	2.524	2/10/17	6:00pm	0	0	0	0	0	
1	20.877	19.945	2/11/17	5:48pm		23	58	1.00	23.97	
2	172.178	168.867	2/12/17	12:43pm	1	19	43	1.82	43.72	
3	222.362	220.225	2/13/17	10:00am	2	16	0	2.67	64.00	
4	180.147	178.524	2/13/17	5:00pm	2	23	0	2.96	71.00	
5	228.235	224.892	2/14/17	2:20pm	3	20	0	3.83	92.00	
6	225.241	222.407	2/15/17	9:46am	4	15	46	4.66	111.77	
7	192.778	189.232	2/15/17	4:30pm	4	22	30	4.94	118.50	
8	197.272	196.796	2/16/17	8:55am	5	14	55	5.62	134.92	
9	194.117	191.77	2/16/17	4:44pm	5	22	44	5.95	142.73	
10	199.939	198.261	2/17/17	10:56am	6	16	56	6.71	160.93	
11	182.647	182.915	2/17/17	4:38pm	6	22	38	6.94	166.63	

Table B.15: Crossflow silver leaching study for ^CAg-NP/CA membrane

Test 1 Chemically Attached Ag-NPs										
sample	Ag 328.068 ppb	Ag 338.289 ppb								
For samples 1-13, time was started at 4:00pm 3/15/17										
			date	time reading	day	hours	minutes	total days	total hours	
blank	1.569	2.456	3/15/17	4:00pm	0	0	0	0.00	0.00	
1	22.15	22.603	3/16/17	8:50am		16	50	0.70	16.83	
2	57.501	55.896	3/16/17	5:20pm	1	20	0	1.83	44.00	
3	59.938	59.737	3/17/17	10:35am	1	18	35	1.77	42.58	
4	68.776	67.304	3/17/17	3:35pm	1	23	35	1.98	47.58	
5	70.767	69.926	3/18/17	10:45am	2	18	45	2.78	66.75	
6	60.522	59.382	3/19/17	10:00am	3	18	0	3.75	90.00	
7	67.223	65.881	3/20/17	8:15am	4	16	15	4.68	112.25	
8	59.197	57.532	3/20/17	7:05pm	5	3	5	5.13	123.08	
9	53.721	53.047	3/21/17	9:08am	5	17	8	5.71	137.13	
10	49.819	49.001	3/21/17	5:12pm	6	1	12	6.05	145.20	
11	52.569	52.115	3/22/17	10:31am	6	18	31	6.77	162.52	
12	53.159	53.4	3/22/17	6:00pm	7	2		7.08	170.00	
13	48.651	47.934	3/22/17	6:00pm	7	2		7.08	170.00	

Table B.16: Crossflow silver leaching study for ^CAg-NP/CA membrane

Test 2 Chemically Attached Ag-NPs										
sample	Ag 328.068 ppb	Ag 338.289 ppb								
For samples 1-15, time was started at 11:51am 3/23/17										
			date	time reading	day	hours	minutes	total days	total hours	
blank	0.486	1.768	3/23/17	11:51am	0	0	0	0.00	0.00	
1	29.056	28.831	3/23/17	5:00pm		5	9	0.21	5.15	
2	76.081	75.338	3/24/17	10:35am		22	44	0.95	22.73	
3	70.671	69.203	3/24/17	11:50am		23	59	1.00	23.98	
4	69.001	68.133	3/24/17	4:30pm	1	4	39	1.19	28.65	
5	66.709	65.081	3/26/17	2:27pm	3	2	36	3.11	74.60	
6	53.691	53.521	3/27/17	9:14am	3	21	23	3.89	93.38	
7	48.686	48.336	3/27/17	4:48pm	4	4	57	4.21	100.95	
8	47.375	46.439	3/28/17	8:21pm	5	8	30	5.35	128.50	
9	46.023	44.733	3/28/17	3:21pm	5	3	30	5.15	123.50	
10	45.676	44.885	3/29/17	9:30am	5	21	39	5.90	141.65	
11	42.333	41.463	3/29/17	5:15pm	6	5	24	6.23	149.40	
12	42.648	43.259	3/30/17	9:06am	6	21	15	6.89	165.25	
13	39.351	38.043	3/30/17	4:32pm	7	4	41	7.20	172.68	
14	37.434	37.309	3/31/17	11:14am	7	23	23	7.97	191.38	
15	35.663	35.992	3/31/17	11:14am	7	23	23	7.97	191.38	

Table B.17: Crossflow silver leaching study for ^CAg-NP/CA membrane

Test 3 Chemically Attached Ag-NPs										
sample	Ag 328.068 ppb	Ag 338.289 ppb								
blank	#VALUE!	1.23								
			date	time reading	day	hours	minutes	total days	total hours	
1	18.805	18.31	4/4/17	4:30pm	0	0	0	0	0	
2	46.18	46.439	4/5/17	8:32am		16	2	0.67	16.03	
3	19.564	19.867	4/5/17	5:20pm	1	0	50	1.03	24.83	
4	24.064	23.494	4/6/17	8:40am	1	16	10	1.67	40.17	
5	21.716	22.695	4/6/17	4:35pm	2	0	5	2.00	48.08	
6	20.751	21.875	4/7/17	9:19am	2	16	49	2.70	64.82	
7	17.585	17.86	4/7/17	6:05pm	3	1	35	3.07	73.58	
8	16.687	18.021	4/9/17	9:55am	4	17	25	4.73	113.42	
9	14.76	14.832	4/9/17	4:30pm	5	2	0	5.08	122.00	
10	15.619	16.812	4/10/17	8:40am	5	16	10	5.67	136.17	
11	14.496	14.67	4/10/17	4:25pm	5	23	55	6.00	143.92	
12	13.926	14.564	4/11/17	10:00am	6	17	30	6.73	161.50	
13	15.454	15.644	4/11/17	5:05pm	7	0	35	7.02	168.58	
14	15.079	15.868	4/12/17	11:40am	7	19	10	7.80	187.17	
15	13.044	14.189	4/12/17	6:27pm	8	1	57	8.08	193.95	
16	14.758	16.246	4/13/17	8:50am	8	16	20	8.68	208.33	

Table B.18: XPS At.% of three ^CAg-NP/CA membrane performed in separate reactions

Total elemental	Atomic %				
	Trial 1	Trial 2	Trial 3	average	std dev.
Carbon	63.11	62.59	65.67	63.79	1.65
Oxygen	31.06	33.09	30.82	31.66	1.25
Nitrogen	3.34	3.21	2.59	1.86	0.40
Sulfur	0.93	0.60	0.50	0.75	0.23
Silver	1.56	0.51	0.42	0.83	0.63

REFERENCES

1. Falkenmark, M., *Rapid Population Growth and Water Scarcity: The Predicament of Tomorrow's Africa*. Population and Development Review, 1990. **16**: p. 81-94.
2. *Managing Water under Uncertainty and Risk*. The United Nations World Water Development Report 4, 2012. **1**.
3. Escobar, I.C.S., Andrea, *Sustainability Science and Engineering*, in *Sustainability Science and Engineering*, C.E. Isabel and I.S. Andrea, Editors. 2010, Elsevier. p. ii.
4. Kallman, E.N., V.A. Oyanedel-Craver, and J.A. Smith, *Ceramic Filters Impregnated with Silver Nanoparticles for Point-of-Use Water Treatment in Rural Guatemala*. Journal of Environmental Engineering, 2011. **137**(6): p. 407-415.
5. Eltawil, M.A., Z. Zhengming, and L. Yuan, *A review of renewable energy technologies integrated with desalination systems*. Renewable and Sustainable Energy Reviews, 2009. **13**(9): p. 2245-2262.
6. Van Der Bruggen, B., et al., *A review of pressure-driven membrane processes in wastewater treatment and drinking water production*. Environmental Progress, 2003. **22**(1): p. 46-56.
7. Andrade, P.F., et al., *Improved antibacterial activity of nanofiltration polysulfone membranes modified with silver nanoparticles*. Water Research, 2015. **81**: p. 333-342.
8. Hausman, R. and I.C. Escobar, *A comparison of silver- and copper-charged polypropylene feed spacers for biofouling control*. Journal of Applied Polymer Science, 2012: p. n/a-n/a.
9. Werber, J.R., C.O. Osuji, and M. Elimelech, *Materials for next-generation desalination and water purification membranes*. Nature Reviews Materials, 2016. **1**(5): p. 16018.
10. Guillen, G.R., et al., *Preparation and Characterization of Membranes Formed by Nonsolvent Induced Phase Separation: A Review*. Industrial & Engineering Chemistry Research, 2011. **50**(7): p. 3798-3817.
11. Sánchez-Márquez, J.A., Fuentes-Ramírez, R., Cano-Rodríguez, I., Gamiño-Arroyo, Z., Rubio-Rosas, E., Kenny, J.M., Rescignano, N., *Membrane Made of Cellulose Acetate with Polyacrylic Acid Reinforced with Carbon Nanotubes and Its Applicability for Chromium Removal*. International Journal of Polymer Science, 2015. **2015**: p. 12.
12. Puls, J., S.A. Wilson, and D. Höltzer, *Degradation of Cellulose Acetate-Based Materials: A Review*. Journal of Polymers and the Environment, 2011. **19**(1): p. 152-165.
13. Palza, H., *Antimicrobial Polymers with Metal Nanoparticles*. International Journal of Molecular Sciences, 2015. **16**(1): p. 2099-2116.
14. I.C. Escobar, E.H., C. Gabelich, F. DiGiano, Y. Le Gouellec, P. Berube, K. Howe, J., et al., *Committee Report: Recent advances and research needs in membrane fouling*. Journal (American Water Works Association), 2005. **97**(8): p. 79-89.
15. Asapu, S., et al., *An investigation of low biofouling copper-charged membranes for desalination*. Desalination, 2014. **338**: p. 17-25.

16. Ben-Sasson, M., et al., *In situ formation of silver nanoparticles on thin-film composite reverse osmosis membranes for biofouling mitigation*. Water Research, 2014. **62**: p. 260-270.
17. Hausman, R. and I.C. Escobar, *A Fourier Transform Infrared Spectroscopic Based Biofilm Characterization Technique and Its Use to Show the Effect of Copper-Charged Polypropylene Feed Spacers in Biofouling Control*, in *Modern Applications in Membrane Science and Technology*. 2011, American Chemical Society. p. 225-237.
18. Flemming, H.C., *Biofouling in water systems--cases, causes and countermeasures*. Appl Microbiol Biotechnol, 2002. **59**(6): p. 629-40.
19. Nguyen, T., F.A. Roddick, and L. Fan, *Biofouling of water treatment membranes: a review of the underlying causes, monitoring techniques and control measures*. Membranes (Basel), 2012. **2**(4): p. 804-40.
20. Zodrow, K., et al., *Polysulfone ultrafiltration membranes impregnated with silver nanoparticles show improved biofouling resistance and virus removal*. Water Res, 2009. **43**(3): p. 715-23.
21. Chede, S. and I.C. Escobar, *Fouling control using temperature responsive N-isopropylacrylamide (NIPAAm) membranes*. Environmental Progress & Sustainable Energy, 2016. **35**(2): p. 416-427.
22. Ferreira, A.M., et al., *High flux microfiltration membranes with silver nanoparticles for water disinfection*. Desalination and Water Treatment, 2015. **56**(13): p. 3590-3598.
23. Daci-Ajvazi, M., et al., *Membrane and Adsorption Processes for Removing of Organics and Inorganics from Urban Wastewaters*. Oriental Journal of Chemistry, 2016. **32**(5): p. 2391-2400.
24. Fabris, R., et al., *Pre-treatments to reduce fouling of low pressure micro-filtration (MF) membranes*. Journal of Membrane Science, 2007. **289**(1-2): p. 231-240.
25. Chou, W.-L., D.-G. Yu, and M.-C. Yang, *The preparation and characterization of silver-loading cellulose acetate hollow fiber membrane for water treatment*. Polymers for Advanced Technologies, 2005. **16**(8): p. 600-607.
26. Glater, J., Hong, S., and Elimelech, M., *The search for a chlorine-resistant reverse osmosis membrane*. Desalination, 1994. **95**: p. 325-345.
27. Kang, G.-d. and Y.-m. Cao, *Development of antifouling reverse osmosis membranes for water treatment: A review*. Water Research, 2012. **46**(3): p. 584-600.
28. Park, S.Y., Chung, J.W., Priestley, R.D., Kwak, S., *Covalent assembly of metal nanoparticles on cellulose fabric and its antimicrobial activity*. Cellulose, 2012. **19**: p. 2141-2151.
29. Sile-Yuksel, M., et al., *Effect of silver nanoparticle (AgNP) location in nanocomposite membrane matrix fabricated with different polymer type on antibacterial mechanism*. Desalination, 2014. **347**: p. 120-130.
30. Prince, J.A., et al., *Synthesis and characterization of PEG-Ag immobilized PES hollow fiber ultrafiltration membranes with long lasting antifouling properties*. Journal of Membrane Science, 2014. **454**: p. 538-548.

31. Sinclair, T., et al., *High-speed water sterilization using silver-containing cellulose membranes*. Nanotechnology, 2014. **25**(30): p. 305101.
32. Stensberg, M.C., et al., *Toxicological studies on silver nanoparticles: challenges and opportunities in assessment, monitoring and imaging*. Nanomedicine (Lond), 2011. **6**(5): p. 879-98.
33. Zhang, H. and V. Oyanedel-Craver, *Evaluation of the Disinfectant Performance of Silver Nanoparticles in Different Water Chemistry Conditions*. Journal of Environmental Engineering, 2012. **138**(1): p. 58-66.
34. Zhang, H., J.A. Smith, and V. Oyanedel-Craver, *The effect of natural water conditions on the anti-bacterial performance and stability of silver nanoparticles capped with different polymers*. Water Res, 2012. **46**(3): p. 691-9.
35. Pulit-Prociak, J. and M. Banach, *Silver nanoparticles – a material of the future...?*, in *Open Chemistry*. 2016. p. 76.
36. Son, W.K., Youk, J.H., and Park, W.H, *Antimicrobial cellulose acetate nanofibers containing silver nanoparticles*. Carbohydrate Polymers, 2006. **65**: p. 430-434.
37. Behra, R., et al., *Bioavailability of silver nanoparticles and ions: from a chemical and biochemical perspective*. Journal of the Royal Society Interface, 2013. **10**(87): p. 20130396.
38. Chen, K.L., et al., *Assessing the colloidal properties of engineered nanoparticles in water: case studies from fullerene C60 nanoparticles and carbon nanotubes*. Environmental Chemistry, 2010. **7**(1): p. 10-27.
39. Huang, J., et al., *Casein-coated Iron Oxide Nanoparticles for High MRI Contrast Enhancement and Efficient Cell Targeting*. ACS applied materials & interfaces, 2013. **5**(11): p. 4632-4639.
40. Zhu, X., et al., *Immobilization of silver in polypropylene membrane for anti-biofouling performance*. Biofouling, 2011. **27**(7): p. 773-786.
41. Association, W.Q., *Silver*. 2015, National Headquarters & Laboratory: Lisle, Illinois.
42. Jain, P. and T. Pradeep, *Potential of silver nanoparticle-coated polyurethane foam as an antibacterial water filter*. Biotechnol Bioeng, 2005. **90**(1): p. 59-63.
43. Yin, J., et al., *Attachment of silver nanoparticles (AgNPs) onto thin-film composite (TFC) membranes through covalent bonding to reduce membrane biofouling*. Journal of Membrane Science, 2013. **441**: p. 73-82.
44. Ulbricht, M., *Advanced functional polymer membranes*. Polymer, 2006. **47**: p. 2217-2262.
45. Escobar, I.C. and S.M.C. Ritchie, *Selected water/wastewater membrane-related presentations from the North American Membrane Society 2007 Annual Meeting*. Environmental Progress, 2008. **27**(2): p. 169-172.
46. Beier, S.P., *Pressure Driven Membrane Processes - 2nd edition*. 2013: BookBoon.
47. Ou, R., Wang, Y., Zhang, H., Wang, H., & Xu, T., *Preparation of high-flux ultrafiltration membranes by blending strongly charged polymer*. Journal of Applied Polymer Science, 2016. **134**(10): p. 1-10.
48. Shon, H.K., et al., *Nanofiltration for water and wastewater treatment – a mini review*. Drinking Water Engineering and Science, 2013. **6**(1): p. 47-53.

49. Yu, S., et al., *Cellulose acetate hollow fiber nanofiltration membrane with improved permselectivity prepared through hydrolysis followed by carboxymethylation*. *Journal of Membrane Science*, 2013. **434**: p. 44-54.
50. Greenlee, L.F., et al., *Reverse osmosis desalination: Water sources, technology, and today's challenges*. *Water Research*, 2009. **43**(9): p. 2317-2348.
51. Peng, W. and I.C. Escobar, *Rejection Efficiency of Water Quality Parameters by Reverse Osmosis and Nanofiltration Membranes*. *Environmental Science & Technology*, 2003. **37**(19): p. 4435-4441.
52. Conlon, W.J., *Water Quality and Treatment, 4th Edition, Chapter 11: Membrane Processes*. Fourth ed. 1990: American Water Works Association.
53. Wenten, I.G., *Ultrafiltration in Water Treatment and Its Evaluation as Pre-treatment for Reverse Osmosis System*.
54. Xu, P., et al., *Critical Review of Desalination Concentrate Management, Treatment and Beneficial Use*. *Environmental Engineering Science*, 2013. **30**(8): p. 502-514.
55. Pressdee, J.R., et al., *Integration of Membrane Filtration Into Water Treatment Systems*. 2006: Awwa Research Foundation/American Water Works Association/IWA Pub.
56. Radcliff, R.Z.A., *Application of Membrane Technology to the Production of Drinking Water*. *Water Conditioning & Purification*, 2004: p. 23-25.
57. Gorey, C. and I.C. Escobar, *N-isopropylacrylamide (NIPAAm) modified cellulose acetate ultrafiltration membranes*. *Journal of Membrane Science*, 2011. **383**(1-2): p. 272-279.
58. Eykamp, W., *Chapter 1 Microfiltration and ultrafiltration*, in *Membrane Science and Technology*, D.N. Richard and S.A. Stern, Editors. 1995, Elsevier. p. 1-43.
59. Van de Witte, P., Dijkstra, P.J., Van den Berg, J.W.A., & Feijen, J., *Phase separation processes in polymer solutions in relation to membrane formation*. *Journal of Membrane Science*, 1996. **117**: p. 1-31.
60. Mulder, M., *Phase Inversion Membranes*. 2000: p. 3331-3346.
61. Bai, H., et al., *The Permeability and Mechanical Properties of Cellulose Acetate Membranes Blended with Polyethylene glycol 600 for Treatment of Municipal Sewage*. *Procedia Environmental Sciences*, 2012. **16**: p. 346-351.
62. Sagle A., F., B., *Fundamentals of Membranes for Water Treatment*. J.A. (Ed.), 2004. **II**(The Future of Desalination in Texas, vol. II. Texas Water Development Board): p. 137-153.
63. López-Ramírez, J.A., M.D.C. Oviedo, and J.M.Q. Alonso, *Comparative studies of reverse osmosis membranes for wastewater reclamation*. *Desalination*, 2006. **191**(1-3): p. 137-147.
64. Ridgway, H.F., M.G. Rigby, and D.G. Argo, *Bacterial Adhesion and Fouling of Reverse Osmosis Membranes*. *Journal (American Water Works Association)*, 1985. **77**(7): p. 97-106.
65. Madigan, M.T., Martinko, J. M., Stahl, D. A., & Clark, D. P., *Brock Biology of Microorganisms*. Thirteenth ed. 2012, San Francisco, CA: Pearson.

66. Kumar, R. and A.F. Ismail, *Fouling control on microfiltration/ultrafiltration membranes: Effects of morphology, hydrophilicity, and charge*. Journal of Applied Polymer Science, 2015. **132**(21): p. n/a-n/a.
67. Abdelrasoul, A., H. Doan, and A. Lohi, *Fouling in Membrane Filtration and Remediation Methods*, in *Mass Transfer - Advances in Sustainable Energy and Environment Oriented Numerical Modeling*, H. Nakajima, Editor. 2013, InTech: Rijeka. p. Ch. 08.
68. Field, R., *Fundamentals of Fouling*, in *Membrane Technology*. 2010, Wiley-VCH Verlag GmbH & Co. KGaA. p. 1-23.
69. Elimelech, M., et al., *Role of membrane surface morphology in colloidal fouling of cellulose acetate and composite aromatic polyamide reverse osmosis membranes*. Journal of Membrane Science, 1997. **127**(1): p. 101-109.
70. Cohen, R.D. and R.F. Probstein, *Colloidal fouling of reverse osmosis membranes*. Journal of Colloid and Interface Science, 1986. **114**(1): p. 194-207.
71. Baker, J.S.D., L.Y., *Biofouling in membrane systems - A review Baker and Dudley*. Desalination, 1998. **118**: p. 81-90.
72. Zaky, A.M., *Characterization of Ultrafiltration Membranes and Effect of Biofouling on Their Water Treatment Performance*. 2011, University of Toledo.
73. Flemming, H.C., et al., *Biofouling—the Achilles heel of membrane processes*. Desalination, 1997. **113**(2): p. 215-225.
74. Ramli, N.S., et al., *The effect of environmental conditions on biofilm formation of Burkholderia pseudomallei clinical isolates*. PLoS One, 2012. **7**(9): p. e44104.
75. Melo, L.F. and T.R. Bott, *Biofouling in water systems*. Experimental Thermal and Fluid Science, 1997. **14**(4): p. 375-381.
76. Pinheiro, M.M., et al., *Surface phenomena and hydrodynamic effects on the deposition of pseudomonas fluorescens*. The Canadian Journal of Chemical Engineering, 1988. **66**(1): p. 63-67.
77. Lehtola, M.J., et al., *The effects of changing water flow velocity on the formation of biofilms and water quality in pilot distribution system consisting of copper or polyethylene pipes*. Water Research, 2006. **40**(11): p. 2151-2160.
78. Rana, D. and T. Matsuura, *Surface Modifications for Antifouling Membranes*. Chemical Reviews, 2010. **110**(4): p. 2448-2471.
79. Wenten, I.G., *Mechanisms and control of fouling in crossflow microfiltration*. Filtration & Separation, 1995. **32**(3): p. 252-253.
80. Ho, W.S.W. and K.K. Sirkar, *Membrane handbook*. 1992, New York: Van Nostrand Reinhold.
81. Varsha, C., Bajpai, S.K. & Navin, C., *Investigation of water vapour permeation and antibacterial properties of nano silver loaded cellulose acetate film*. International Food Research Journal, 2010. **17**: p. 623-639.
82. Abdo, H.S., et al., *Antibacterial effect of carbon nanofibers containing Ag nanoparticles*. Fibers and Polymers, 2014. **14**(12): p. 1985-1992.
83. Hadrup, N. and H.R. Lam, *Oral toxicity of silver ions, silver nanoparticles and colloidal silver – A review*. Regulatory Toxicology and Pharmacology, 2014. **68**(1): p. 1-7.

84. Choi, O. and Z. Hu, *Size dependent and reactive oxygen species related nanosilver toxicity to nitrifying bacteria*. Environ. Sci. Technol., 2008. **42**: p. 4583.
85. Yang, Y., et al., *Potential nanosilver impact on anaerobic digestion at moderate silver concentrations*. Water Res, 2012. **46**(4): p. 1176-84.
86. Reidy, B., et al., *Mechanisms of Silver Nanoparticle Release, Transformation and Toxicity: A Critical Review of Current Knowledge and Recommendations for Future Studies and Applications*. Materials, 2013. **6**(6): p. 2295.
87. Palleroni, N.J., *Pseudomonas classification A new case history in the taxonomy of Gram-negative bacteria*. Antonie van Leeuwenhoek, 1993. **64**: p. 231-251.
88. Buettner, G.R. and B.A. Jurkiewicz, *Catalytic Metals, Ascorbate and Free Radicals: Combinations to Avoid*. Radiation Research, 1996. **145**(5): p. 532-541.
89. Choi, O., et al., *Role of sulfide and ligand strength in controlling nanosilver toxicity*. Water Research, 2009. **43**(7): p. 1879-1886.
90. Zhao, S., et al., *Poly(ether sulfone)/Polyaniline Nanocomposite Membranes: Effect of Nanofiber Size on Membrane Morphology and Properties*. Industrial & Engineering Chemistry Research, 2014. **53**(28): p. 11468-11477.
91. Sotto, A., et al., *Effect of nanoparticle aggregation at low concentrations of TiO₂ on the hydrophilicity, morphology, and fouling resistance of PES–TiO₂ membranes*. Journal of Colloid and Interface Science, 2011. **363**(2): p. 540-550.
92. Lee, D.Y., et al., *Silver nanoparticles dispersed in electrospun polyacrylonitrile nanofibers via chemical reduction*. Journal of Sol-Gel Science and Technology, 2010. **54**(1): p. 63-68.
93. Pastoriza-Santos, I.L.-M., Luis, *Synthesis of Silver Nanoprisms in DMF*. Nano Letters, 2002. **2**(8): p. 903-905.
94. Yang, H.-L., J.C.-T. Lin, and C. Huang, *Application of nanosilver surface modification to RO membrane and spacer for mitigating biofouling in seawater desalination*. Water Research, 2009. **43**(15): p. 3777-3786.
95. Cao, X., et al., *Immobilization of silver nanoparticles onto sulfonated polyethersulfone membranes as antibacterial materials*. Colloids and Surfaces B: Biointerfaces, 2010. **81**(2): p. 555-562.
96. Kwon, J., Yoon, S.H., Lee, S.S., Seo, K.W. & Shim, I., *Preparation of Silver Nanoparticles in Cellulose Acetate Polymer and the Reaction Chemistry of Silver Complexes in the Polymer*. Bull. Korean Chem. Soc., 2005. **26**(5): p. 837-840.
97. Benaglia, M., et al., *Poly(glycidyl methacrylate): a highly versatile polymeric building block for post-polymerization modifications*. Polym. Chem., 2013. **4**(1): p. 124-132.
98. Hausman, R., T. Gullinkala, and I.C. Escobar, *Development of copper-charged polypropylene feedspacers for biofouling control*. Journal of Membrane Science, 2010. **358**(1–2): p. 114-121.
99. McEwan, K.A., et al., *Dual-functional materials via CCTP and selective orthogonal thiol-Michael addition/epoxide ring opening reactions*. Polymer Chemistry, 2013. **4**(8): p. 2608.

100. Zheng, Y., et al., *Polypropylene nonwoven fabrics with conformal grafting of poly(glycidyl methacrylate) for bioseparations*. Journal of Membrane Science, 2010. **364**(1-2): p. 362-371.
101. Wang, J., et al., *Preparation, Characterization and Properties of Cellulose Acetate-Grafted-Poly(glycidyl methacrylate) Copolymers*. Journal of Macromolecular Science: Pure & Applied Chemistry, 2015. **52**(3): p. 226-233.
102. Groarke, R. and D. Brabazon, *Methacrylate Polymer Monoliths for Separation Applications*. Materials, 2016. **9**(6): p. 446.
103. Quiles, F., F. Humbert, and A. Delille, *Analysis of changes in attenuated total reflection FTIR fingerprints of Pseudomonas fluorescens from planktonic state to nascent biofilm state*. Spectrochim Acta A Mol Biomol Spectrosc, 2010. **75**(2): p. 610-6.
104. Boscher, N.D., Hilt, F., Duday, D., Frache, G., Fouquet, T., & Choquet, P., *Atmospheric Pressure Plasma Initiated Chemical Vapor Deposition Using Ultra-Short Square Pulse Dielectric Barrier Discharge*. Plasma Process. Polym., 2015. **12**: p. 66-74.
105. Beverly, S., S. Seal, and S. Hong, *Identification of surface chemical functional groups correlated to failure of reverse osmosis polymeric membranes*. Journal of Vacuum Science & Technology A: Vacuum, Surfaces, and Films, 2000. **18**(4): p. 1107-1113.
106. Dang, H.T., Narbaitz, R.M., Matsuura, T., and Khulbe, K.C., *A Comparison of Commercial and Experimental Ultrafiltration Membranes via Surface Property Analysis and Fouling Tests*. Water Qual. Res. J., 2006. **41**(1): p. 84-93.
107. Atkinson, M.J. and C. Bingman, *Elemental composition of commercial sea salts*. Journal of Aquaculture and Aquatic Sciences, 1997. **8**(2): p. 39-43.
108. Kester, D.R., et al., *Preparation of Artificial Seawater*. Limnology and Oceanography, 1967. **12**(1): p. 176-179.
109. Pilson, M.E.Q., *An Introduction to the Chemistry of the Sea*. 1998: Prentice Hall.
110. Oyanedel-Craver, V. and J.A. Smith, *Sustainable colloidal-silver-impregnated ceramic filter for point-of-use water treatment*. Environ. Sci. Technol., 2008. **42**: p. 927.
111. Meng, L.M., et al., *A dual mechanism single-component self-healing strategy for polymers*. Journal of Materials Chemistry, 2010. **20**(29): p. 6030-6038.
112. del Valle Martínez de Yuso, M., et al., *Chemical Surface, Thermal and Electrical Characterization of Nafion Membranes Doped with IL-Cations*. Applied Sciences, 2014. **4**(2): p. 195.
113. María Arsuaga, J., et al., *Influence of the type, size, and distribution of metal oxide particles on the properties of nanocomposite ultrafiltration membranes*. Journal of Membrane Science, 2013. **428**: p. 131-141.
114. Huang, L. and J.R. McCutcheon, *Impact of support layer pore size on performance of thin film composite membranes for forward osmosis*. Journal of Membrane Science, 2015. **483**: p. 25-33.
115. Polyakov, Y.S. and A.L. Zydney, *Ultrafiltration membrane performance: Effects of pore blockage/constriction*. Journal of Membrane Science, 2013. **434**: p. 106-120.

116. Takeshima, T., et al., *DNA/Ag Nanoparticles as Antibacterial Agents against Gram-Negative Bacteria*. *Nanomaterials* (Basel), 2015. **5**(1): p. 284-297.

VITA

July 2017

Conor Gary Lee Sprick

Place of Birth

Rockford, Illinois, USA

Education

Bachelor of Science, Professional Chemistry
University of Evansville, Evansville, Indiana, 2011-2015

Professional Positions

Graduate Research Assistant, 2015-2017
College of Engineering, University of Kentucky, Lexington, KY

Graduate Teaching Assistant, Fall 2016
College of Engineering, University of Kentucky, Lexington, KY

Teaching Assistant, Fall 2015, Spring 2016
Department of Chemistry, University of Kentucky, Lexington, KY

Research and Development Chemist Intern, Summer 2015
Kester: An ITW Company, Itasca, IL

Materials Analysis Intern, Summer 2014
Berry Plastics Corporation, Evansville, IN

Chemist Intern, Summer 2013
Red Spot Paint & Varnish Co. Inc., Evansville, IN

Scholastic and Professional Honors

“Student Poster Presentation Award” *Advanced Membrane Technology VII: An ECI Conference*, Sept. 11-16, 2016, Cork, Ireland.

University of Evansville

- Ridgeway Vanderburgh Scholarship
- Wuetherich Family Scholarship
- Dean’s List 2012

University of Evansville, NCAA Division I Men’s Swimming & Diving Team

- CSCAA All-America Team honors, 2014-2015
- All-MAC Honorable Mention Team, 2013-2015
- MAC Honor Rolls, 2013-2015
- Voted Most Improved Veteran Male, 2015
- Aired on “Inside Aces Athletics,” Nov. 11, 2012 at University of Evansville (<https://www.youtube.com/watch?v=fDV6WAF6jyo>)